USAFETAC/PR--92/003



# SAC CONTRAIL FORMATION STUDY

by

Captain Brian M. Bjornson



MAY 1992





USAF
ENVIRONMENTAL TECHNICAL
APPLICATIONS CENTER

Scott Air Force Base, Illinois 62225-5438

## REVIEW AND APPROVAL STATEMENT

USAFETAC/PR--92/003, *SAC Contrail Formation Study*, May 1992, has been reviewed and is approved for public release. There is no objection to unlimited distribution of this document to the public at large, or by the Defense Technical Information Center (DTIC) to the National Technical Information Service (NTIS).

WALTER F. MILLER, Major, USAF
Chief of Aerospace Sciences

BRIAN M. BJORNSON, Capt, USAF
Writer/Analyst

FOR THE COMMANDER

WALTER S. BURGMANN
Scientific and Technical Information
Program Manager
*19 May 1992*

**A NOTE TO OUR CUSTOMERS--**

**The authors and editors of this publication welcome feedback, both positive and negative. We value your opinion. Please let us know what you like and do not like about our products. Also, please let us know if your address has changed, or if you wish to receive more or fewer copies of AWS and USAFETAC technical documents in primary distribution. If you need more copies of this document, or if you know of someone else who might be interested in this or other AWS/USAFETAC publications, let us know that too. Call, write, or FAX:**

**USAFETAC/LDE**
**Scott AFB, IL 62225-5458**

**DSN 576-6648 Commercial 618 256-6648 Fax 3772**

## REPORT DOCUMENTATION PAGE

2. Report Date: May 1992

3. Report Type: Project Report

4. Title: SAC Contrail Formation Study

6. Authors: Capt Brian M. Bjornson

7. Performing Organization Name and Address: USAF Environmental Technical Applications Center (USAFETAC/DNO), Scott AFB, IL 62225-5458

8. Performing Organization Report Number: USAFETAC/PR--92/003

12. Approved for public release; distribution unlimited

13. Abstract: This report documents the results of a study that compares the Appleman contrail forecasting method used at the Air Force Global Weather Central (AFGWC) with the SAC method using pilot report (PIREP) data collected by SAC/DOW between March 1990 and July 1991. The study resulted in development of two other contrail forecasting techniques. The first (ETACFCST) was developed using discriminant analysis schemes to obtain "best fit" curves of contrail formation as a function of altitude and temperature, or altitude, temperature, and vertical motion. Statistics showed ETACFCST to be better than either the Appleman or SAC contrail prediction curves. But another technique developed near the end of the study incorporated aircraft engine type as a factor for the first time. The new engine-specific contrail forecasting technique is recommended as a replacement for the Appleman method used at AFGWC.

14. Subject Terms: CLIMATOLOGY, CLOUDS, CIRRUS CLOUDS, FORECASTING, ALGORITHMS, CONDENSATION TRAILS, CONTRAILS, EXHAUST TRAILS, VAPOR TRAILS, AIRCRAFT ENGINES, AIRCRAFT TYPES

15. Number of Pages: 48

17. Security Classification of Report: Unclassified

18. Security Classification of this Page: Unclassified

19. Security Classification of Abstract: Unclassified

20. Limitation of Abstract: UL

**Standard Form 298**

# PREFACE

This report documents the results of USAFETAC Project 910548, performed for SAC/DOW by USAFETAC's Operations Applications Development section (DNO). Capt Brian M. Bjornson was the writer/analyst.

When SAC/DO identified a weakness in forecasting contrails, SAC/DOW asked USAFETAC for help; specifically, to compare the Appleman method used at the Air Force Global Weather Central (AFGWC) with the SAC/DOW contrail prediction curves, using PIREP data that had been collected by SAC/DOW between March 1990 and July 1991.

In addition to making the comparison requested above, USAFETAC used the SAC/DOW PIREP data to develop a new contrail forecasting technique, called "ETACFCST." Discriminant analysis schemes were used to obtain "best-fit" curves of contrail formation as a function of altitude and temperature, or altitude, temperature, and vertical motion. Statistics showed the new method to be better than either the Appleman or SAC/DOW contrail prediction curves above and below 40,000 feet. Later in the study, Capt Jeffery L. Peters (SAC/DOW) modified the SAC/DOW contrail prediction curve to include an aircraft engine "fuel-to-air" ratio. USAFETAC then used discriminant analysis techniques to determine the best-fit curve of contrail formation as a function of *aircraft engine type*. These algorithms proved superior to the ETACFCST algorithm both above and below 40,000 feet.

USAFETAC therefore recommends that the ETACFCST contrail algorithms, modified to include an aircraft engine type factor, replace the Appleman technique as the AWS contrail prediction algorithm used to forecast contrails.

# CONTENTS

## FIGURES

## TABLES

# 1. INTRODUCTION

**1.1 Background.** In 1989, SAC/DO found a problem with Air Weather Service (AWS) contrail forecasting in that the Appleman contrail forecasting algorithm used by the Air Force Global Weather Central (AFGWC) provided an unacceptable contrail detection probability. AFGWC's inability to forecast contrails to an acceptable degree of accuracy was thought to unnecessarily expose high-flying aircraft to detection. After several other inconclusive studies, SAC/DOW asked USAFETAC (in May 1991) to compare the Appleman and SAC/DOW contrail prediction curves, using a new SAC-provided PIREP database containing 6,815 PIREPS collected by SAC aircrews. Using the new database, which had less bias than the one provided in 1989, USAFETAC developed a new contrail forecasting technique by assuming that the critical temperature for forecasting contrail formation is a function of flight level (or pressure) and vertical motion.

**1.2 Related Studies.** In 1953, Herbert Appleman constructed curves showing the critical temperature for contrail formation as a function of pressure, relative humidity (RH), and the amount of air entrained into aircraft exhaust, regardless of aircraft type, fuel, or power settings. But since RH values from radiosonde reports are often suspect (especially at low temperatures), AFGWC uses RH *assumptions* in the Appleman technique--this will be discussed later. Appleman concluded that in a dry environment, contrails form at very low temperatures, whereas in a more humid environment, they can form at higher temperatures. More recent work in contrail forecasting is documented in USAFETAC/PR-90/003, *SAC Contrail Forecasting Algorithm Validation Study*, by Major Walter F. Miller (1990). Miller used an older database of 463 PIREPS collected by SAC aircrews between 1984 and 1987. He evaluated the SAC/DOW contrail forecasting algorithm (which is pressure independent) and compared it with three RH assumptions using Appleman's algorithm. He found that TROPFCST (an Appleman algorithm in which RH is determined using AFGWC RH assumptions) had a slightly higher contrail forecasting skill than the SAC/DOW algorithm. However, Miller points out that the PIREP dataset used in his study was biased in that 90% of the PIREPS included contrail reports. As a result, the data favored a pessimistic contrail algorithm and overforecasted contrails. Miller's study showed the need for acquiring a database with a balanced number of contrail and no-contrail observations. See Section 2, "Data."

**1.3 Methodology.** The project was divided into several parts:

- Validate temperature data in the SAC PIREP database with High-Resolution Analysis System (HIRAS) temperature data.
- Calculate vertical velocity from HIRAS data using the kinematic method described in AWS/TR-83/001 and use it to quantify vertical velocity from the SAC PIREP database.
- Provide statistical analyses of the original SAC PIREP database (PIREP temperature and vertical motion) and the quality-controlled SAC PIREP database (HIRAS temperature and vertical motion).
- Develop a new contrail forecasting technique.

We used the original SAC/DOW PIREP data and verified it with HIRAS data. We developed algorithms to forecast contrails based on temperature, flight level, and vertical motion at the PIREP location. Finally, comparative statistics for the Appleman, SAC/DOW, and USAFETAC contrail prediction curves were tabulated. Algorithm limitations, such as in their application to certain types of aircraft and engines, were worked out later in the project; see 3.4 and 4.9.

**1.4 Results.** Study results are given in three parts:

- Results for contrail formation *at or below* 40,000 feet. Below 40,000 feet, ETACFCST had better skill and a higher probability of contrail detection than Appleman.
- Results for contrail formation *above* 40,000 feet. Above 40,000 feet, ETACFCST had better skill and a lower false alarm rate than Appleman, but offered a lower probability of contrail detection.
- Results for contrail formation based on aircraft engine type.

**1.5 Recommendations.** Based on the results, we recommend that the algorithms in Appendix D, modified to include aircraft engine type as a factor, replace the Appleman contrail forecasting technique now in use at AFGWC.

## 2. DATA

**2.1 PIREP Database Contents and Limitations.** The SAC PIREP database contained 6,815 PIREPS collected by SAC aircrews between 8 March 1990 and 18 July 1991. Each PIREP was composed of the observation number, date, time, latitude and longitude, flight level, contrail formation (yes/no), temperature, sign of vertical motion at the PIREP level, and results (hit/miss) of the SAC/DOW and Appleman techniques. SAC/DOW estimated the sign (+/-) of the vertical motion by examining 300-mb constant pressure analyses. Upward motion was assumed at all levels between the base of a trough and the apex of the upstream ridge; downward motion was assumed between the apex of a ridge and the base of the upstream trough. According to SAC/DOW, some PIREPS above 40,000 feet may contain biased reports of "non-contrails." Several crews reported no contrails at their flight levels above 40,000 feet. However, crews at lower altitudes reported seeing thin contrails from the higher aircraft. The crews at the higher altitudes were apparently unable to see their own contrails, possibly because of glare. The new database, then, may contain erroneous "no-contrail" reports above 40,000 feet.

***2.1.1 Dependent Data.*** About 80% of the PIREPs (5,464 of 6,815) were kept for a dependent dataset. Nearly 3% (137) of the 5,464 had missing or incorrect dates, times, or flight levels; this left 5,327 useable observations in the dependent dataset. More than 80% (4,294) of the 5,327 were at or below 40,000 feet, and 26% (1,110) of these reported contrails. Above 40,000 feet, more than 60% (626 of 1,033) contained contrail reports. The 1,033 PIREPs from above 40,000 feet contained missing latitude and longitude data and also lacked estimates of the vertical motion sign since vertical motion above 40,000 feet is close to zero (it is assumed to be zero at about 75 mb).

Figure 1 shows the locations of more than 95% of the dependent data at or below 40,000 feet. Dependent data above 40,000 feet couldn't be plotted because of missing latitude and longitude values.

***2.1.2 Independent Data.*** 1,351 of the 6,815 PIREPs were chosen at random for an independent dataset; after QC, the number was reduced to 1,341. About 83% (1,110) of the 1,341 were at or below 40,000 feet; 231 were above 40,000 feet. More than 29% of the PIREPs (325 of 1,110) at or below 40,000 feet contained contrail reports. Above 40,000 feet, 71% (165 of 231) reported contrails. Figure 2 shows the locations for more than 95% of the independent data at or below 40,000 feet. Independent data above 40,000 feet couldn't be plotted because of missing latitude and longitude values.

**2.2 HIRAS Data.** The High Resolution Analysis System (HIRAS) used in the Advanced Weather Analysis and Prediction System (AWAPS) at AFGWC was originally designed to provide improved data for computerized flight plans. Essentially, HIRAS provides only a coarse approximation of the atmosphere. It is optimized for large-scale upper-air flow, not for smaller scale synoptic and mesoscale patterns. It produces global upper-air analyses archived on a 2.5 by 2.5 degree latitude/longitude grid. Data for mandatory levels between the surface and 10 mb can be obtained. The HIRAS model uses observations from land stations, ships, buoys, aircraft, RAOBs, PIBALs, rocketsondes, and satellites. HIRAS variables used in this study were temperature, pressure, u- and v-components of the wind, and tropopause height and pressure. An error field that gives an estimate of the error for each variable at all grid points is carried with HIRAS (see AWS/TN-86/001 for a detailed description of AWAPS).

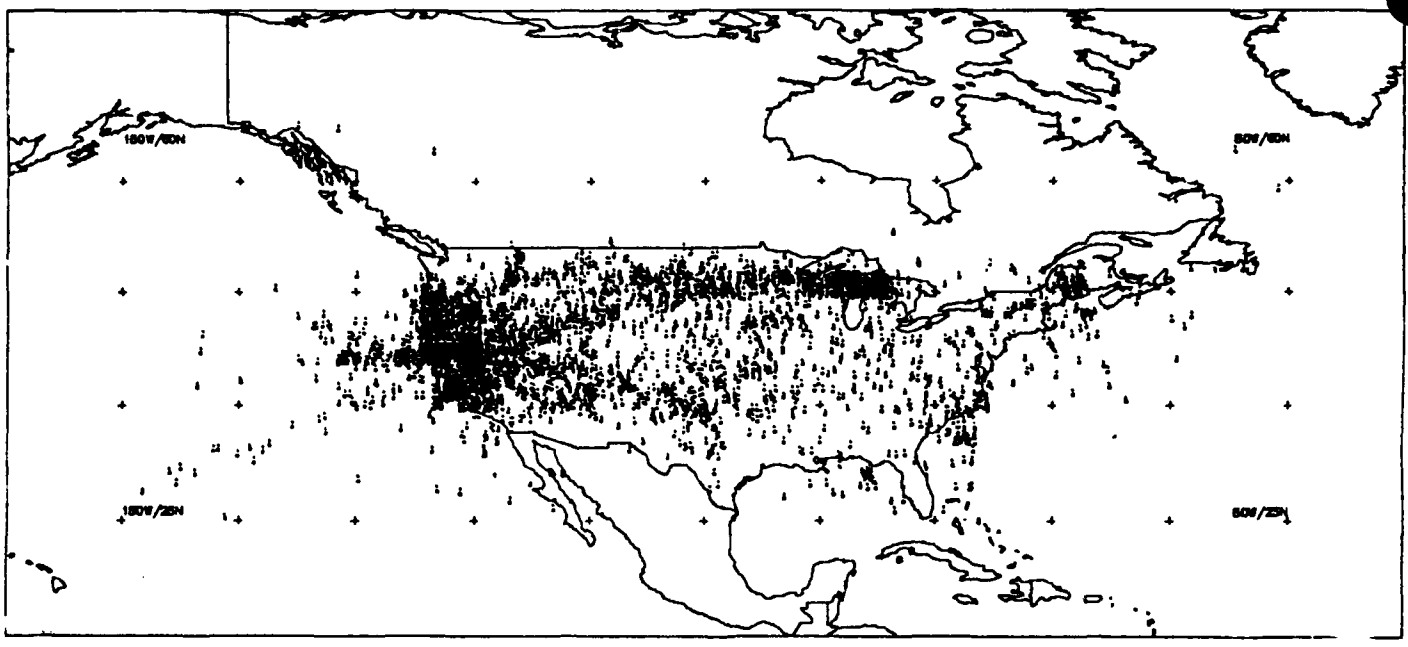

**Figure 1.** Location of over 95 percent of the *dependent* data at/below 40,000 feet.

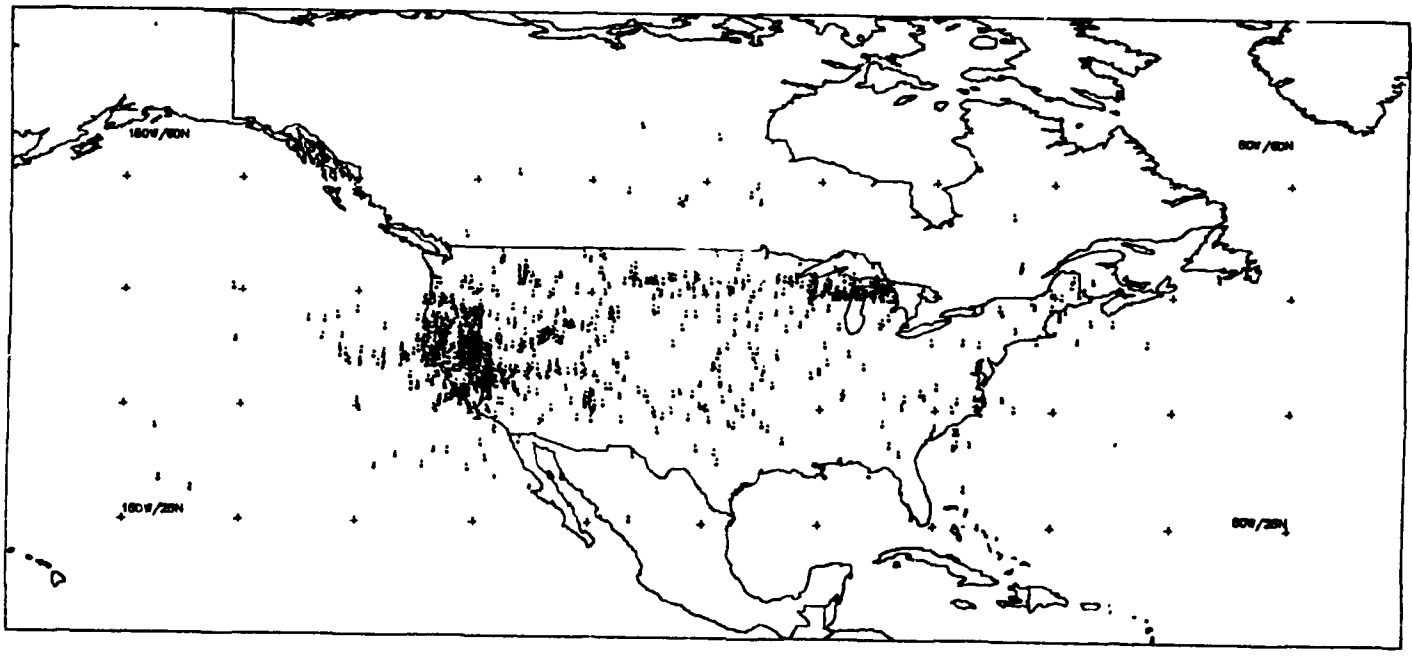

**Figure 2.** Location of over 95 percent of the *independent* data at/below 40,000 feet.

## 3. METHODOLOGY

**3.1 Calculating Temperature and Temperature Error.** Software was developed to calculate temperature (and temperature error) at the PIREP location using HIRAS data.

***3.1.1 Ensuring Consistency Between PIREP and HIRAS Data.*** I/J latitude and longitude values in HIRAS were converted to the nearest half degree. Flight levels from the SAC PIREP database, in hundreds of feet ($Z_F$), were converted to meters ($Z_M$) (Equation 1) and then to pressure ($p$, in mb) (Equation 2 or 3), as shown below:

$$Z_M = \frac{(Z_F \times 100)}{3.281} \qquad (1)$$

If $Z_M$ is less than or equal to 11,000 meters, then:

$$p = 1013.25 \left[1 - \left(\frac{Z_M}{44330.77}\right)\right]^{5.26} \qquad (2)$$

If the height is between 11,000 and 20,000 meters, then:

$$p = \frac{226.32}{e^{\left[\frac{(Z_M - 11000)}{6341.62}\right]}} \qquad (3)$$

***3.1.2 Estimating HIRAS Temperatures Between Data Points.*** The horizontal bi-linear interpolation equation shown below (from AWS/TR-83/001, Equations 4-9) was applied three times. Temperatures (in degrees Celsius) were interpolated to the PIREP location for the standard pressure level above and below each PIREP; that is, if a PIREP was recorded at 350 mb, temperatures ($T$, Equation 4) were determined at 300 and 400 mb).

$$T = T_i + \left[\frac{(T_{i+1} - T_i) \times (S - X_i)}{X_{i+1} - X_i}\right] \qquad (4)$$

where:

$T$ is the temperature at the required point

$T_i$ is the temperature at grid point $i$

$T_{i+1}$ is the temperature at grid point $i+1$

$X_i$ and $X_{i+1}$ are distances (meters) between the grid points and an arbitrary point

$S$ is the distance of the required point from the arbitrary point (depending on location of PIREP)

$S1$ is distance from point A along line AB until it intersects the horizontal line extending from the PIREP location (point $P$).

$T$ is the temperature at a distance $S1$

$X_{i+1}$ and $S$ are defined relative to $X_i$ ($X_i=0$) and are dependent upon their latitude.

Since the distance between each degree of longitude varies depending on location, the Clarke spheroid of 1866 (Smithsonian, 1984) was used to determine the length of 1 degree of the meridian, depending on the latitude.

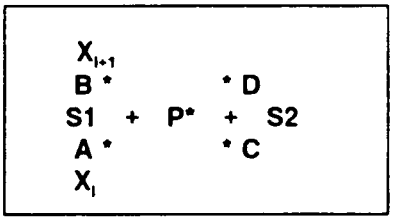


**Figure 3.** Horizontal bilinear interpolator diagram.

The value of temperature at *S2* is obtained using *C* as *i* and *D* as *i+1* and Equation 4. Using calculations of temperature at *S1* and *S2*, Equation 5 was used to calculate the temperature at the latitude and longitude position of each PIREP ($T_p$) at the standard levels above and below each PIREP:

$$T_p = T_{s1} + \left[\frac{(T_{s2} - T_{s1}) \times (P - S1)}{S2 - S1}\right] \qquad (5)$$

where *P* is the distance from *S1* to point *P* and *S2* is the distance from *S1*.

***3.1.3 Determining Temperature at PIREP Pressure Level.*** A vertical log-pressure interpolator (Equation 6) was used to determine temperature (*T*) at the pressure level (*P*) of each PIREP (AWS/TR-83/001, Equations 4-9).

$$T = T_i + \left[\frac{(T_{i+1} - T_i) \times (\ln p - \ln p_i)}{\ln p_{i+1} - \ln p_i}\right] \qquad (6)$$

where:

$T$ is the temperature at the pressure level $(p)$ where the PIREP was made

$T_i$ is the temperature at pressure $p_i$

$T_{i+1}$ is the temperature at pressure $p_{i+1}$.

Temperatures at 400 and 300 mb ($T_i$ and $T_{i+1}$, respectively) were taken directly from bi-linear horizontal interpolation results (see 3.1.2); $p$ is also known. See Figure 4.

***3.1.4 Determining Temperatures.*** The root mean square error for HIRAS temperature is 2-3° C. An error field carried with HIRAS gives an estimate of temperature error for each point. PIREP temperatures were compared to HIRAS temperatures. When the absolute value of their difference was greater than the absolute value of the error plus 1° C, the data was flagged (i.e., identified as HIRAS temperatures in the dataset) and comparison statistics were generated. Original PIREP temperatures and calculated HIRAS temperatures were included in the final dataset.

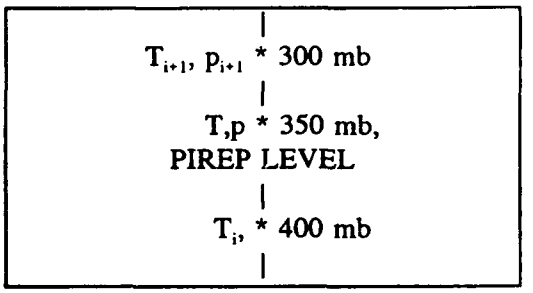


**Figure 4.** Vertical log-pressure interpolator diagram.

**3.2 Calculating Vertical Velocity from HIRAS Data.** We developed software to calculate the vertical velocity at the PIREP location (using HIRAS data) by applying the kinematic method described in AWS/TR-83/001. Both HIRAS vertical velocity and PIREP (original) vertical velocity were included in the final dataset. According to Duffield and Nystrom (1983), the kinematic method (based on the continuity equation) for estimating vertical velocity is preferred over the adiabatic method or omega equation. After the first integration of the continuity equation from the surface to pressure level $p_1$, the new lower boundary value for vertical velocity $(w)$ becomes the bottom value for the next integration. This results in a problem because of the inaccuracy of the winds, together with the cumulative error in the integration processes. To eliminate the problem, Nystrom suggested starting the integration process at 75 mb (where $w = 0\ ms^{-1}$) and working downward through the atmosphere.

***3.2.1 Vertical Velocity Calculation Between Pressure Levels.*** Equation 7 was used to calculate vertical velocity between each standard level from 75 mb to the surface (standard levels are 100, 150, 200, 250, 300, 400, 500, 700, 850, and 1,000 mb). (Note: The

equation below was derived from Equations 4-7, AWS/TR-83/001. Lt Col Nystrom, co-author of that publication, modified the equation for use in this study).

$$w_{k-1} = \left[\frac{(\varrho_k \times w_k)}{\varrho_{k-1}}\right] - \left\{\left[\frac{1}{(\varrho_{k-1} \times g)}\right] \times \left[\left(\frac{d_x u}{d}\right) + \left(\frac{d_y v}{d}\right)\right] \times [100(p_k - p_{k-1})]\right\} \quad (7)$$

where:

$w_{k-1}$ is the vertical velocity ($ms^{-1}$) half a level below the standard level

$w_k$ is the vertical velocity half a level above the standard level ($w_k$ = 0 $ms^{-1}$ at 75 mb)

$\varrho_k$ is the density ($kgm^{-3}$) at level $k$ ($\varrho = (100*p)/RT$)

$p$ is the pressure in mb

$T$ is the temperature K

$R$ (the dry gas constant) is 287 $J°K^{-1}kg^{-1}$)

$\varrho_{k-1}$ is the density at level $k$-$1$

$g$ is acceleration due to gravity ($g$ = 9.81 $ms^{-2}$)

$s^{-1}$), $d_x u$ (the divergence) is the difference of $u$ (u-comp of horizontal wind, $ms^{-1}$), linearly interpolated to the center of the north/south line between grid points, in the east/west line

$d_y v$ is the difference of $v$ in the north/south line

$d$ is the distance in meters between grid points and varies depending on latitude location of PIREP

$p_k - p_{k-1}$ is the difference in pressure (mb) between pressure at level $k$ and level $k$-$1$.

The calculation is started at 75 mb, with $w_k$ assumed to be zero. The divergence terms are calculated from the 100-mb level data to produce the vertical velocity at 125 mb. This process is repeated downward through the atmosphere to the surface.

***3.2.2 Vertical Velocity Calculation at the PIREP Pressure Level.*** A vertical log-pressure interpolator (similar to the one described in 3.1.3) was used to calculate vertical velocity at the pressure level of the PIREP. For example, if a PIREP was taken at 350 mb, vertical velocity at the PIREP location was determined using a vertical log-pressure interpolator with wind and pressure inputs from 300 and 400 mb. Vertical velocities were quality-controlled to ensure that there were no gross values (in general, values were between -0.08 and +0.08 m/s). Only the sign of the vertical velocity was kept in the final dataset, since actual values were questionable. The sign of the vertical velocities calculated from HIRAS was compared with the sign of the original vertical velocity. Both dependent and independent datasets used in this study contain vertical velocities calculated from HIRAS and PIREP data.

### 3.2.3 *Vertical Motion--Kinematic Method vs 300-mb Analysis.*

The success or failure of the kinematic method in providing reliable results depends on how well horizontal winds in HIRAS represent actual atmospheric conditions. HIRAS, unfortunately, describes only the synoptic scale upper-airflow because its resolution is only 2.5 by 2.5 degrees. The kinematic method produces the best results where a dense network of observed winds is available. Whether or not this method is superior to "eyeballing" 300-mb analyses is unknown. Although the resolution on the NGM 300-mb analysis (60 nm) is better than HIRAS, vertical interpolation was not used in the eyeballing process to determine vertical motion at the altitude (pressure) the PIREP was taken. The eyeballing method assumes the sign of the estimated vertical velocity at 300 mb represents the sign of the actual vertical velocity at the PIREP location.

**3.3 Statistics.** All statistics included in this report were prepared from two combinations of temperature and vertical motion data extracted from the final SAC PIREP database.

- PIREP temperature and PIREP vertical motion data (original).
- HIRAS temperature and HIRAS vertical motion data (calculated).

Standardized normal variables (Z test statistics) were computed to determine the equality between the percent frequencies of contrail occurrences using upward and downward motion. If the Z statistic was greater than a certain value, the frequency of contrails associated with upward motion is significantly different from percent frequencies associated with downward motion.

### 3.3.1 *Sensitivity Analyses of Temperature vs Altitude.*

Each sensitivity analysis gives the number of occurrences/non-occurrences and percent frequency of altitude vs temperature. Temperatures were stratified in 5° C increments; altitude was stratified in 5,000-feet increments.

### 3.3.2 *The USAFETAC Contrail Prediction Curve.*

A discriminant analysis (DA) scheme was used to obtain a "best-fit" curve (USAFETAC contrail prediction curve) of contrail formation as a function of altitude vs temperature and of altitude vs temperature vs vertical motion. Discriminant analysis involves deriving the linear combination of two or more independent variables that will best discriminate between the categories of the dependent variable (in DA, the dependent variable must be categorical; i.e., yes/no. Discriminant analysis is the appropriate statistical technique for testing the hypothesis that the group means of two or more groups are equal (Hair et. al., 1987). To accomplish this, each independent variable is multiplied by its corresponding weight and their products are added together. The result is a single composite discriminant score for all observations within a particular group. The Fisher discriminant function (Afifi and Clark, 1984) is written:

$$Z = a_1 X_1 + a_2 X_2 \qquad (8)$$

where $a_1$ and $a_2$ are the discriminant weights, $X_1$ and $X_2$ are the independent variables, and $Z$ is the discriminant score. In this study, altitude (PIREP flight level) and temperature are the *independent* variables; contrail (vs no-contrail) formation is the *dependent* variable. A separate DA was completed using dependent data classified by:

- upward motion (data at or below 40,000 feet)
- downward motion (data at or below 40,000 feet)
- all data at or below 40,000 feet (upward, downward, and missing vertical motion)
- all data above 40,000 feet (missing vertical motion)

Separate discriminant analyses were accomplished for PIREP (original) and HIRAS (calculated) data. As requested by the customer, separate discriminant analyses were also completed for each 5,000-foot increment between FL 200 and 400, using HIRAS data. These

results were compared with results obtained by using a single discriminant equation to forecast contrails at or below 40,000 feet.

***3.3.3 Tropopause Height and Pressure Data Extracted from HIRAS Database.*** This data was needed to estimate relative humidity for use in applying the Appleman and SAC/DOW contrail prediction curves using original and calculated temperature and vertical motion data. In both curves, RH is assumed to be 40% in the troposphere, 70% within 300 meters of the tropopause, and 10% in the stratosphere (see USAFETAC/PR-90/003 for a detailed description of these curves). Contingency tables were created using SAC PIREP data (original PIREP and calculated HIRAS data) and applying the Appleman and SAC/DOW curves. Statistics (described in 3.3.5) generated using the different prediction curves were then compared with statistics applying the USAFETAC contrail prediction curve.

***3.3.4 Dependent Data Less Than or Equal to 40,000 Feet*** was plotted on scatter diagrams with the Appleman, SAC/DOW, and USAFETAC (ETACFCST) contrail prediction curves overlaid. Twelve diagrams were prepared; six using PIREP (original) data, and six using HIRAS (calculated) data. Each dataset (PIREP, HIRAS) was used to plot data containing records with:

- upward motion only
- downward motion only
- upward, downward, and missing vertical motion (all motions)

The three categories were divided further so that the Appleman and SAC/DOW curves with different RH assumptions could be plotted and analyzed. The customer requested that the Appleman and SAC/DOW curves for 100% RH and for 40% RH be plotted on separate diagrams. Contrail occurrences were denoted by a plus sign; non-occurrences, by a diamond. Because several observations of contrails and no-contrails were overprinted (hiding multiple observations at a single point), a random number generator was used to add (or subtract) small increments of temperature and altitude from the actual value. Since vertical motion is missing above 40,000 feet, data above 40,000 feet was plotted on scatter diagrams using PIREP data only. Two scatter diagrams were completed with the USAFETAC, Appleman, and SAC/DOW contrail prediction curves overlaid. As requested by the customer, one plot depicted Appleman and SAC/DOW curves assuming 10% RH; the other assumed 100% RH.

**3.3.5 Skill Scores.** The Heidke skill score (HSS) was used to assess the skill or accuracy of the results. The equation used is:

$$HSS = \frac{(F - D)}{(T - D)} \qquad (9)$$

where $F$ is the number of *correct forecasts*, $T$ is the *total number of forecasts*, and $D$ is the *number of forecasts expected to be correct* based on chance. The equation for $D$ is:

$$D = \frac{[(C1 \times R1) + (C2 \times R2) + \ldots + (Cn \times Rn)]}{T} \qquad (10)$$

where:

$n$ is the number of contingencies

$C$ and $R$ are the sums of the columns and rows taken from the contingency table shown in Figure 5

$T$ is the total number of forecasts

The HSS ranges from -1 (no skill) to 1 (total accuracy). In meteorological applications, an HSS between 0.30 and 0.40 is considered satisfactory, and an HSS greater than 0.40 typically indicates good skill. According to Appleman (1960), the HSS does not measure forecasts against a true standard. From Equations 9 and 10, the expected number of correct forecasts based on pure chance depends on the number of forecasts for each category issued. Appleman indicates that the standard

should be independent of forecasts being evaluated, and suggests replacing the variable *"D"* in Equation 9 with the number of observations in the category that is observed most frequently. His critical skill index (CSI) is given by:

$$CSI = \frac{X}{[X + (T_f - X) + (T_o - X)]} \qquad (11)$$

where $X$ is the number of correct forecasts, $T_f$ is the number of event forecasts, and $T_o$ is the total number of event occurrences. Woodcock (1976) stated that the Heidke skill score is "trial-dependent"; that is, any trial in which the events and non-events are not equally represented (e.g., contrail occurrences vs non-occurrences) is biased. Woodcock suggested using Hanssen and Kuipers' (1968) discriminant "V" score:

$$VDS = \frac{AD - BC}{[(A + B) \times (C + D)]} \qquad (12)$$

where VDS is the discriminant V-score, ranging from -1 (no skill) to 1 (total accuracy). *A, B, C,* and *D* are elements from a "2x2" contingency table shown in Figure 5:

| CONTRAILS | | |
|---|---|---|
| | FCST NO | FCST YES |
| OBS NO | A | B |
| OBS YES | C | D |

**Figure 5.** Contingency Table.

According to Woodcock, VDS provides an impartial and satisfactory measure of forecasting accuracy for scientific purposes and should therefore be weighted highest when interpreting results. Goldsmith (1989) recommended using probability of detection (POD), false alarm ratio (FAR), and critical skill index (CSI) to supplement skill scores. POD is the number of correct forecasts of an event divided by the total number of times the event occurred. FAR is the number of times an event was incorrectly forecast to occur divided by the total number of times the event was forecast. All measures discussed so far are included in Section 4, "Results."

***3.3.6 The "p-value" (PVAL)*** is one of the statistics generated from the "chi-square" test, which is used to determine if the *observed* frequency distributions differ significantly from *expected* frequency distributions (those which result from chance). The chi-square test shows only whether or not two frequency distributions differ significantly from each other. When chi-square is larger than certain limits, the observed frequency distribution is significantly different from the expected distributions (i.e., the results are not by chance). The level of significance, or PVAL, is used to determine the weight of the difference between observed and expected distributions. P-values less than or equal to 0.01 indicate that results are almost certainly significant.

When the p-value is 0.05, there is one chance in twenty that the forecast could have been made by chance--this is still considered a reliable result. P-values greater than 0.05 usually indicate that results are *not* significantly different from chance. For this study, p-values less than or equal to 0.05 were considered to indicate statistically significant results.

***3.4 Engine-Specific Contrail Forecasting Algorithm.*** Just before publication of this document, SAC/DOW changed its contrail prediction algorithm to include the fuel-to-air ratio of aircraft engines found in certain SAC aircraft; that is, the algorithms were changed to make contrail forecasting engine-specific. The statistics in Appendix D, Tables 1-5, support the use of engine-specific algorithms for forecasting contrails.

***3.4.1 Engine Classification.*** Engines were classified as "*high*-bypass" (KC-135R), "*low*-bypass" (KC-10), or "*non*-bypass" (KC-135A, B-52G, U-2).

***3.4.2 Verification.*** USAFETAC verified the new engine-specific algorithms using USAFETAC's empirical (discriminant analysis) method for forecasting contrails with PIREP data sorted by aircraft type as follows: KC-135A, 322 PIREPS; KC-135R, 334 PIREPS; B-52G, 340 PIREPS; and U-2, 1,110 PIREPS. Since there was no data available for the KC-10, the low-bypass engine algorithm could not be verified. Statistics based on discriminant analysis techniques were generated and compared with statistics produced using the new SAC/DOW contrail curves based on Applemans's theoretical algorithm--see Figure 4.9.

## 4. RESULTS.

**4.1 HIRAS vs PIREP Temperature.** Calculated HIRAS temperatures replaced original PIREP temperatures in about 60% (2,564 of 4,294) of all dependent observations at or below 40,000 feet. PIREP and HIRAS temperatures were retained for use in separate discriminant analyses and scatter diagrams. HIRAS temperatures could not be determined above 40,000 feet because these PIREPS lacked reports of latitude and longitude necessary for the horizontal and vertical interpolators used to calculate HIRAS temperature at the PIREP level.

**4.2 HIRAS vs PIREP Vertical Motion.** The sign of the vertical velocity (+/-) between calculated HIRAS velocities and original PIREP velocities differed in nearly 38% (1,615 of 4,294) of all dependent observations at or below 40,000 feet. In 21% (910 of 4,294) of these cases, estimates of upward motion from 300-mb analyses (original data) were calculated as *downward* vertical motion from HIRAS data; more than 16% (705 of 4,294) of downward motion estimates from 300-mb analyses were calculated as *upward* motion from HIRAS. Ninety-two percent (1,480 of 1,615) of HIRAS and PIREP vertical velocity differences occurred when the estimated HIRAS vertical velocity was close to zero (within +/- 0.005 m/s). Both HIRAS and PIREP vertical motions (sign only) were retained for use in separate discriminant analyses and scatter diagrams, which will be discussed later.

**4.3 Sensitivity Analyses of Temperature vs Altitude.** Tables 1 through 5 depict the number of occurrences/non-occurrences and percent frequency of occurrences/non-occurrences of contrails (above and below 40,000 ft) as a function of temperature and altitude. Tables 1 to 3 show results using PIREP data; Tables 4 and 5 depict results using HIRAS. Regardless of the data used (PIREP or HIRAS), our results support Appleman's theory that the potential for contrails increases as temperature decreases. Although Appleman considered the effects of relative humidity on contrail formation, he did not analyze the effects of vertical velocity.

***4.3.1 PIREP Data At/Below 40,000 Feet.*** Z test statistics for PIREP data indicate that differences in frequency of occurrence between upward and downward vertical motion were significantly different (see 4.3.1.2).

***4.3.1.1 PIREP Temperatures and All Vertical Motion Data (upward, downward, and missing vertical motion).*** Contrails occurred in only 27 of 509 (5%) of all observations between FL 200/240, in relatively warm air. Contrail frequency increased to 21% (383 of 1,811) between FL 250/290 and 33% (558 of 1,682) between FL 300 and 340. Between FL 350 and 400, contrail frequency increased to 61% (140 of 230) overall. When temperatures were -50° C or less, contrail frequency increased to over 73% between FL 250 and 340 and to about 77% (109 of 141) between FL 350 and 400. Finally, at the lowest temperatures (less than -55° C), frequency of contrails increased to over 85% (112 of 131) between FL 300 and 400.

***4.3.1.2 PIREP Temperatures; Upward Motion (Table 1) vs Downward Motion (Table 2).*** Between FL 250 and 340, frequency of contrails using upward vertical motion was about twice the frequency for downward motion (29 vs 14% between FL 250 and 290 and 44 vs 22% between FL 300 and 340). Between FL 350 and 400, frequency of contrails was 74% (73 of 99) for upward motion and only 54% (59 of 109) for downward motion. As temperatures decreased to -50° C or below between FL 250 and 340, contrail frequency increased to 83 percent (110 of 132) using upward motion, compared with 63% (89 of 142) using downward motion. At altitudes between FL 350 and 400 with temperatures below -50° C, contrails occurred in 83% (53 of 64) of observations associated with upward motion as compared to 66% (51 of 77) for downward motion.

**TABLE 1.** Number of occurrences/non-occurrences and percent frequency of occurrences/non-occurrences of contrails at/below 40,000 feet as a function of PIREP temperature, PIREP *upward* vertical motion, and altitude (flight level).

| | 200/240 Contrail | | | | 250/290 Contrail | | | | 300/340 Contrail | | | | 350/400 Contrail | | | |
|---|---|---|---|---|---|---|---|---|---|---|---|---|---|---|---|---|
| | No | | Yes | | No | | Yes | | No | | Yes | | No | | Yes | |
| Temp at FLTLVL | N | % | N | % | N | % | N | % | N | % | N | % | N | % | N | % |
| -64 to -60 | . | . | . | . | . | . | . | . | . | . | 1 | 100 | . | . | 6 | 100 |
| -59 to -55 | . | . | . | . | . | . | . | . | 1 | 5 | 21 | 95 | 6 | 22 | 21 | 78 |
| -54 to -50 | . | . | . | . | 3 | 14 | 19 | 86 | 21 | 19 | 88 | 81 | 5 | 17 | 25 | 83 |
| -49 to -45 | . | . | . | . | 23 | 28 | 58 | 72 | 77 | 39 | 129 | 61 | 9 | 38 | 15 | 63 |
| -44 to -40 | 2 | 50 | 2 | 50 | 68 | 44 | 85 | 56 | 154 | 62 | 96 | 38 | 4 | 50 | 4 | 50 |
| -39 to -35 | 8 | 80 | 2 | 20 | 185 | 81 | 42 | 19 | 160 | 81 | 37 | 19 | 1 | 100 | . | . |
| -34 to -30 | 28 | 84 | 2 | 5 | 195 | 86 | 33 | 14 | 62 | 86 | 10 | 14 | . | . | . | . |
| -29 to -25 | 41 | 95 | 2 | 5 | 119 | 85 | 21 | 15 | 8 | 89 | 1 | 11 | 1 | 50 | 1 | 50 |
| -24 to -20 | 65 | 92 | 6 | 8 | 34 | 87 | 5 | 13 | . | . | . | . | . | . | . | . |
| > -20 | 57 | 95 | 3 | 5 | 5 | 100 | . | . | . | . | . | . | . | . | . | . |
| ALL | 202 | 92 | 17 | 8 | 632 | 71 | 264 | 29 | 483 | 56 | 374 | 44 | 26 | 27 | 72 | 73 |

**TABLE 2.** Number of occurrences/non-occurrences and percent frequency of occurrences/non-occurrences of contrails at/below 40,000 feet as a function of PIREP temperature, PIREP *downward* vertical motion, and altitude (flight level).

| | 200/240 Contrail | | | | 250/290 Contrail | | | | 300/340 Contrail | | | | 350/400 Contrail | | | |
|---|---|---|---|---|---|---|---|---|---|---|---|---|---|---|---|---|
| | No | | Yes | | No | | Yes | | No | | Yes | | No | | Yes | |
| Temp at FLTLVL | N | % | N | % | N | % | N | % | N | % | N | % | N | % | N | % |
| -64 to -60 | . | . | . | . | . | . | . | . | 1 | 33 | 2 | 67 | 1 | 14 | 6 | 86 |
| -59 to -55 | . | . | . | . | 1 | 33 | 2 | 67 | 6 | 22 | 21 | 78 | 3 | 10 | 28 | 90 |
| -54 to -50 | 1 | 100 | . | . | 4 | 40 | 6 | 60 | 46 | 41 | 66 | 59 | 13 | 43 | 17 | 57 |
| -49 to -45 | . | . | . | . | 53 | 67 | 25 | 33 | 148 | 76 | 46 | 24 | 15 | 71 | 6 | 29 |
| -44 to -40 | 3 | 100 | . | . | 159 | 80 | 39 | 20 | 260 | 92 | 22 | 8 | 13 | 87 | 2 | 13 |
| -39 to -35 | 22 | 88 | 3 | 12 | 198 | 93 | 15 | 7 | 92 | 93 | 7 | 7 | 3 | 100 | . | . |
| -34 to -30 | 39 | 98 | 1 | 3 | 167 | 92 | 15 | 8 | 37 | 95 | 2 | 5 | 1 | 100 | . | . |
| -29 to -25 | 42 | 100 | . | . | 105 | 95 | 6 | 5 | 1 | 100 | . | . | . | . | . | . |
| -24 to -20 | 72 | 97 | 2 | 3 | 39 | 91 | 4 | 9 | . | . | . | . | . | . | . | . |
| > -20 | 60 | 97 | 2 | 3 | 2 | 67 | 1 | 3 | . | . | . | . | . | . | . | . |
| ALL | 239 | 97 | 8 | 3 | 728 | 86 | 118 | 14 | 591 | 78 | 166 | 22 | 49 | 45 | 59 | 55 |

***4.3.2 PIREP Temperature Data Above 40,000 Feet, No Vertical Motion Data Available.*** As shown in Table 3, frequency of contrails above 40,000 feet was highest (100%, 20 PIREPS) between 410 and 440 feet, but decreased to 75% (501 of 667) between FL 440 and 650. Above FL 650, contrails occurred in only 30% (104 of 346) of observations even though frequency was near 75% (28 of 37) when temperatures were -70° C or lower. When all flight levels above 40,000 feet were considered, contrails occurred in 92% (327 of 354) of all observations when temperatures were -70° C or less.

**TABLE 3.** Number of occurrences/non-occurrences and percent frequency of occurrences/non-occurrences of contrails above 40,000 feet as a function of PIREP temperature and altitude (flight level).

| Temp at FL/FLVL | 410/440 Contrail Yes | | 450/490 Contrail | | | | 500/540 Contrail | | | | 550/590 Contrail | | | | 600/640 Contrail | | | | 650/690 Contrail | | | |
|---|---|---|---|---|---|---|---|---|---|---|---|---|---|---|---|---|---|---|---|---|---|---|
| | | | No | | Yes | | No | | Yes | | No | | Yes | | No | | Yes | | No | | Yes | |
| | N | % | N | % | N | % | N | % | N | % | N | % | N | % | N | % | N | % | N | % | N | % |
| < = -80 | . | . | . | . | . | . | . | . | 2 | 100 | . | . | . | . | . | . | 2 | 100 | . | . | . | . |
| -79 to -75 | . | . | . | . | . | . | . | . | 3 | 100 | 1 | 20 | 4 | 80 | 2 | 1 | 63 | 97 | . | . | 3 | 100 |
| -74 to -70 | 2 | 100 | . | . | 1 | 100 | . | . | 2 | 100 | 3 | 27 | 8 | 73 | 12 | 5 | 212 | 95 | 9 | 26 | 25 | 74 |
| -69 to -65 | 5 | 100 | 1 | 14 | 6 | 86 | . | . | . | . | 4 | 44 | 5 | 56 | 96 | 35 | 179 | 65 | 159 | 64 | 64 | 31 |
| -64 to -60 | 6 | 100 | 2 | 29 | 5 | 71 | 1 | 100 | . | . | . | . | . | . | 81 | 87 | 6 | 13 | 78 | 94 | 5 | 6 |
| -59 to -55 | 6 | 100 | 1 | 33 | 2 | 67 | 1 | 100 | . | . | . | . | . | . | 1 | 50 | 1 | 50 | 5 | 63 | 3 | 38 |
| -54 to -50 | 1 | 100 | . | . | . | . | . | . | . | . | . | . | . | . | . | . | . | . | . | . | . | . |
| ALL | 20 | 100 | 4 | 22 | 14 | 78 | 2 | 22 | 7 | 78 | 8 | 32 | 17 | 68 | 152 | 25 | 463 | 75 | 281 | 70 | 105 | 30 |

### *4.3.3 HIRAS Data At/Below 40,000 Feet.*

Z test statistics for HIRAS data indicate that differences in frequency of occurrence between upward and downward vertical motion were *not* significantly different, except for results at flight levels between 250 and 290 feet (see 4.3.3.2).

***4.3.3.1 HIRAS Temperatures and All Vertical Motion Data.*** Results using HIRAS temperatures and all vertical motion data were similar to results using PIREP data (see 4.3.1.1). Contrail frequency increased between 20,000 feet (5%) and 40,000 feet (60%). Frequency of contrails ranged from 72 to 86% between FL 250 and 400 when temperatures were -50° C or less.

***4.3.3.2 HIRAS Temperatures; Upward (Table 4) vs Downward (Table 5) Motion.*** Although results using either HIRAS or PIREP data coupled with all vertical motions are nearly identical (compare 4.3.1.1 with 4.3.3.1), when HIRAS upward vs downward vertical motion data were compared with PIREP data (see 4.3.1.2), the results were much different. Between FL 250 and 340, frequency of contrails was 28% (462 of 1,632) using upward vertical motion and 26% (479 of 1,857) using downward motion. Between FL 350/400, frequency of contrails was 64% (81 of 127) for downward motion versus 57% (59 of 103) using upward motion. When PIREP data was used between FL 200 and 400, the frequency of contrails using upward motion was about twice as high as that found when using downward motion (35% vs 18%). However, when HIRAS data is used, frequency using upward motion is 29%, compared to 25% for downward motion. The differences in techniques used to estimate the sign of the vertical velocity is probably the major reason for these differences. Also, the original PIREP database contained 206 records with missing vertical velocity estimates; as a result, there are 206 fewer observations used in the PIREP dataset for comparing upward vs downward vertical motions and their relationship with contrail formation.

**TABLE 4.** Number of occurrences/non-occurrences and percent frequency of occurrences/non-occurrences of contrails at/below 40,000 feet as a function of HIRAS temperature, HIRAS *upward* vertical motion, and altitude (flight level).

| | 200/240 Contrail | | | | 250/290 Contrail | | | | 300/340 Contrail | | | | 350/400 Contrail | | | |
|---|---|---|---|---|---|---|---|---|---|---|---|---|---|---|---|---|
| | No | | Yes | | No | | Yes | | No | | Yes | | No | | Yes | |
| Temp at FLTLVL | N | % | N | % | N | % | N | % | N | % | N | % | N | % | N | % |
| -69 to -65 | . | . | . | . | . | . | . | . | . | . | 1 | 100 | . | . | . | . |
| -65 to -60 | . | . | . | . | . | . | . | . | . | . | 1 | 100 | . | . | 4 | 100 |
| -59 to -55 | . | . | . | . | . | . | . | . | 3 | 14 | 19 | 86 | 3 | 14 | 18 | 86 |
| -54 to -50 | . | . | . | . | . | . | 3 | 100 | 25 | 26 | 72 | 74 | 17 | 40 | 26 | 60 |
| -49 to -45 | . | . | 2 | 100 | 20 | 32 | 42 | 68 | 122 | 63 | 71 | 37 | 14 | 64 | 8 | 36 |
| -44 to -40 | 3 | 100 | . | . | 96 | 62 | 60 | 38 | 197 | 75 | 66 | 25 | 9 | 75 | 3 | 25 |
| -39 to -35 | 10 | 91 | 1 | 9 | 143 | 81 | 34 | 19 | 164 | 85 | 29 | 15 | . | . | . | . |
| -34 to -30 | 27 | 90 | 3 | 10 | 215 | 87 | 33 | 13 | 33 | 83 | 7 | 18 | . | . | . | . |
| -29 to -25 | 41 | 100 | . | . | 117 | 88 | 16 | 12 | . | . | . | . | . | . | . | . |
| -24 to -20 | 54 | 95 | 3 | 5 | 39 | 83 | 8 | 17 | . | . | . | . | . | . | . | . |
| > -20 | 85 | 96 | 4 | 4 | . | . | . | . | . | . | . | . | . | . | . | . |
| ALL | 220 | 94 | 13 | 6 | 630 | 76 | 196 | 24 | 544 | 67 | 266 | 33 | 43 | 42 | 59 | 58 |

**TABLE 5.** Number of occurrences/non-occurrences and percent frequency of occurrences/non-occurrences of contrails at/below 40,000 feet as a function of HIRAS temperature, HIRAS *downward* vertical motion, and altitude (flight level).

| | 200/240 Contrail | | | | 250/290 Contrail | | | | 300/340 Contrail | | | | 350/400 Contrail | | | |
|---|---|---|---|---|---|---|---|---|---|---|---|---|---|---|---|---|
| | No | | Yes | | No | | Yes | | No | | Yes | | No | | Yes | |
| Temp at FLTLVL | N | % | N | % | N | % | N | % | N | % | N | % | N | % | N | % |
| -64 to -60 | . | . | . | . | . | . | . | . | . | . | . | . | . | . | 4 | 100 |
| -59 to -55 | . | . | . | . | . | . | . | . | 4 | 19 | 17 | 81 | 6 | 15 | 33 | 85 |
| -54 to -50 | . | . | . | . | 4 | 27 | 11 | 73 | 44 | 34 | 85 | 66 | 15 | 33 | 30 | 67 |
| -49 to -45 | . | . | . | . | 33 | 41 | 47 | 59 | 154 | 58 | 112 | 42 | 19 | 61 | 12 | 39 |
| -44 to -40 | . | . | 2 | 100 | 143 | 71 | 58 | 29 | 228 | 81 | 52 | 19 | 6 | 86 | 1 | 14 |
| -39 to -35 | 11 | 85 | 2 | 15 | 212 | 88 | 30 | 12 | 134 | 88 | 19 | 12 | . | . | . | . |
| -34 to -30 | 41 | 93 | 3 | 7 | 215 | 89 | 26 | 11 | 16 | 70 | 7 | 30 | . | . | . | . |
| -29 to -25 | 44 | 94 | 3 | 6 | 145 | 93 | 11 | 7 | . | . | . | . | . | . | . | . |
| -24 to -20 | 63 | 95 | 3 | 5 | 44 | 92 | 4 | 8 | . | . | . | . | . | . | . | . |
| > -20 | 103 | 99 | 1 | 1 | 2 | 100 | . | . | . | . | . | . | . | . | . | . |
| ALL | 262 | 95 | 14 | 5 | 798 | 81 | 187 | 19 | 580 | 67 | 292 | 33 | 46 | 37 | 80 | 63 |

**4.4 Discriminant Analyses and Scatter Diagrams.** The best-fit curves of contrail formation as functions of temperature vs altitude and of temperature vs altitude vs vertical motion using both PIREP and HIRAS data are described below. Results are given for "at/below 40,000 feet" and "above 40,000 feet." Appendix A compares the skill and accuracy of the SAC/DOW, Appleman, and U.S. AFETAC contrail prediction curves. Scatter diagrams (Figures 6-11) are also shown, with the different prediction curves overlaid (SAC/DOW requested Appleman and SAC/DOW contrail prediction curves be plotted using 40% and 100% RH for data at/below 40,000 feet; RH is assumed equal to 10% and 100% for plots above 40,000 feet).

***4.4.1 PIREP Temperature Data At/Below 40,000 Feet.*** The scatter diagrams in Figures 6 through 11 depict contrail formation as functions of altitude and temperature, or altitude, temperature, and vertical motion, using original PIREP data. SAC/DOW and Appleman curves are plotted assuming either 100 or 40% RH. Associated statistics are provided in Tables A-1 through A-3 in Appendix A. P-values (not shown) indicate statistically significant results, regardless of the type of vertical motion.

***4.4.1.1 Upward, Downward, and Missing Vertical Motion (all PIREP data).*** Scatter diagrams for all PIREPS at/below 40,000 feet are shown in Figures 6 and 7. The Appleman and SAC/DOW

curves with RH = 100% (Figure 6) and RH = 40% (Figure 7) are overlaid. Also shown is the USAFETAC best-fit curve based on the discriminant equation:

$$TCRIT = -28.21 - (0.0391 \times FL) \quad (13)$$

where *TCRIT* is the flight level temperature (° C) and *FL* is the flight level in hundreds of feet (e.g., 300 = 30,000 feet). If the actual temperature is less than *TCRIT*, contrails are inferred. Statistical results (Appendix A, Table A-1) support the USAFETAC contrail prediction curve (ETACFCST), even though its percent correct (COR) is about 10% lower than for the other curves. All three skill scores (VDS, HSS, CSI) are higher for ETACFCST, especially the discriminant V-score (VDS). Although ETACFCST has a high false alarm rate (FAR), the probability of detection (POD) is considerably higher than Appleman or SAC/DOW. Equation 13, therefore, can be used to forecast contrails based on *FL* and *TEMPFL*. The chi-square statistical test indicates the model (equation) produces statistically significant results (PVAL < 0.05). Figure 7 provides a "quick-look" comparison of the contrail prediction curves assuming 40% RH, which is realistic for the troposphere. Appleman and SAC/DOW curves do not distinguish between contrails and no-contrails well because many actual occurrences of contrails are depicted as non-contrails, resulting in a low POD.

***4.4.1.2 Upward Vertical Motion.*** Scatter diagrams for upward motion PIREPS at/below 40,000 feet are shown in Figures 8 and 9. Appleman and SAC/DOW curves are overlaid with the RH assumption as described in 4.4.1.1. The ETACFCST discriminant curve for forecasting contrails is plotted using the discriminant equation:

$$TCRIT = -24.59 - (0.0495 \times FL) \quad (14)$$

All skill scores for ETACFCST (Table A-2) are safisfactory, and indicate higher skill than Appleman and SAC/DOW curves. POD and COR are excellent for ETACFCST, but the FAR is over 40%. Results for Appleman are slightly better than results for SAC/DOW.

***4.4.1.3 Downward Vertical Motion.*** Scatter diagrams for downward motion PIREPS at/below 40,000 feet are shown in Figures 10 and 11. Appleman, SAC/DOW, and ETACFCST curves are overlaid. The ETACFCST discriminant equation for forecasting contrails associated with downward motion is shown below:

$$TCRIT = -28.58 - (0.04626 \times FL) \quad (15)$$

Skill scores (Table A-3) show that ETACFCST and Appleman are both skillful in forecasting contrails associated with downward vertical motion. However, nearly twice as many contrails are detected using ETACFCST and Appleman (79 vs 42% POD). Unfortunately, the false alarm rate is twice as high for ETACFCST than for Appleman (67 vs 31%).

***4.4.2 PIREP Temperature Data Above 40,000 Feet.*** The scatter diagrams for all PIREPS above 40,000 feet are shown in Figures 12 and 13. Appleman and SAC/DOW curves assuming 100% and 10% RH are overlaid (Figures 12 and 13, respectively). ETACFCST discriminant curves are plotted based on the equation:

$$TCRIT = -31.59 - (0.0572 \times FL) \quad (16)$$

Statistics (Table a-4) indicate that Appleman and ETACFCST are skillful and fairly accurate. ETACFCST has higher skill (VDS=0.60) and lower FAR (11.6%) than Appleman (VDS=0.47 FAR=23.0) but Appleman has a better POD (91.4 vs 75.4%). The SAC/DOW curve lacks skill mainly because it cannot distinguish between contrails and no-contrails. Equation 16 can be used to forecast contrails based on flight-level and flight-level temperature. If the forecast flight-level temperature is less than TEMPFL as calculated from Equation 16, then contrails should be forecast. The chi-square statistical test indicates that this equation is statistically significant (PVAL<0.05). These results indicate

that Equation 16 is reliable for use in predicting contrail formation above 40,000 feet. The discriminant analysis curve (Figure 13) is similar to the Appleman curve, which is considerably warmer (about 3° C) near 41,000 feet and over 4° C warmer at 70,000 feet). Figure 13 also indicates that the Appleman curve does not distinguish well between contrails and "no contrails," because many actual non-occurrences of contrails are depicted as occurrences. The data does not support the SAC/DOW curve, which indicates that contrails occur when the air temperature is less than or equal to -52° C.

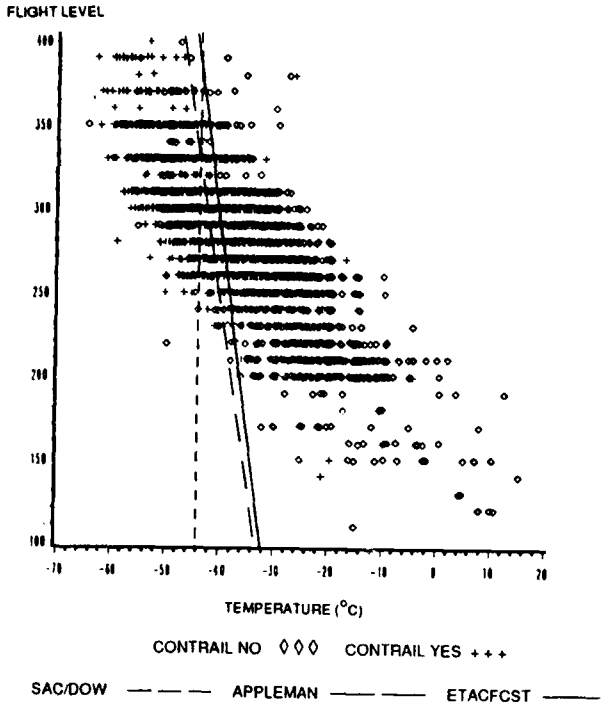


**Figure 6.** Scatter diagram: All PIREP data at/below 40,000 feet, *all vertical motion data, RH=100%* for Appleman and SAC/DOW curves.

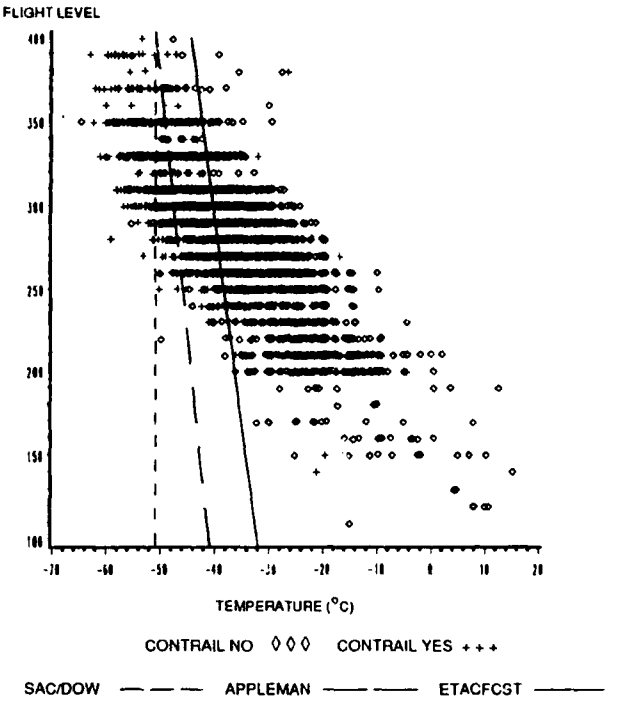


**Figure 7.** Scatter diagram: All PIREP data at/below 40,000 feet, *all vertical motion data, RH=40%* for Appleman and SAC/DOW curves.

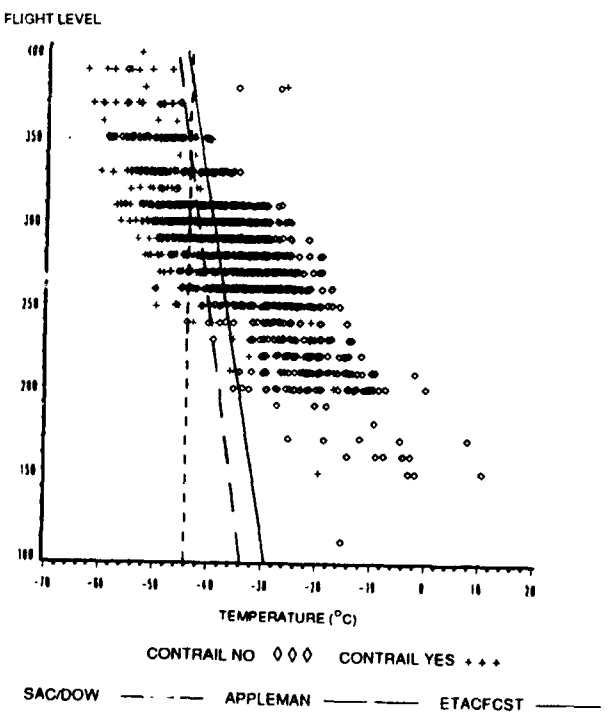


**Figure 8.** Scatter diagram: All PIREP data at/below 40,000 feet, *upward vertical motion only, RH=100%* for Appleman and SAC/DOW curves.

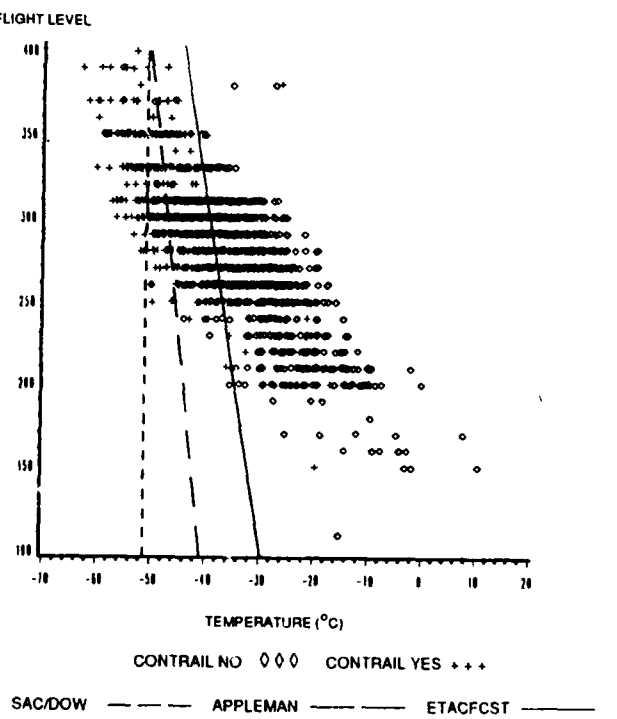


**Figure 9.** Scatter diagram: All PIREP data at/below 40,000 feet, *upward vertical motion only, RH=40%* for Appleman and SAC/DOW curves.

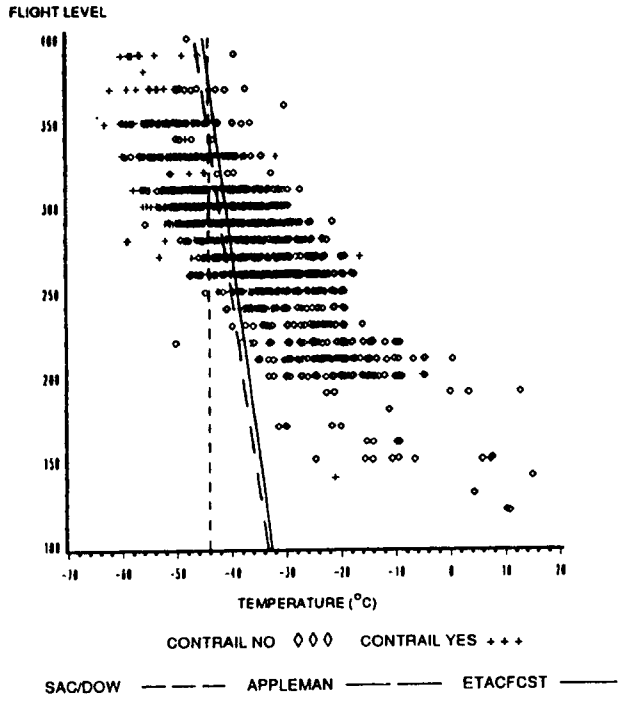


**Figure 10.** Scatter diagram: All PIREP data at/below 40,000 feet, using *downward vertical motion* only, *RH-100%* for Appleman and SAC/DOW curves.

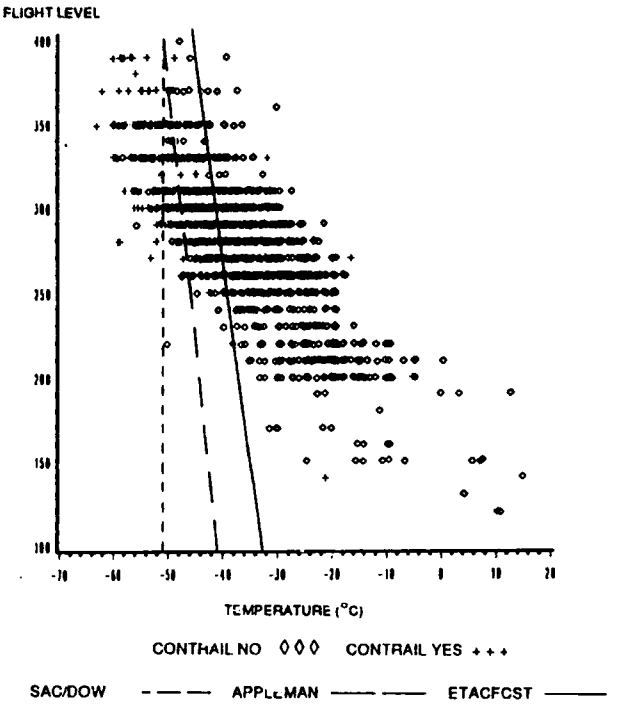


**Figure 11.** Scatter diagram: All PIREP data at/below 40,000 feet, using *downward vertical motion* only, *RH=40%* for Appleman and SAC/DOW curves.

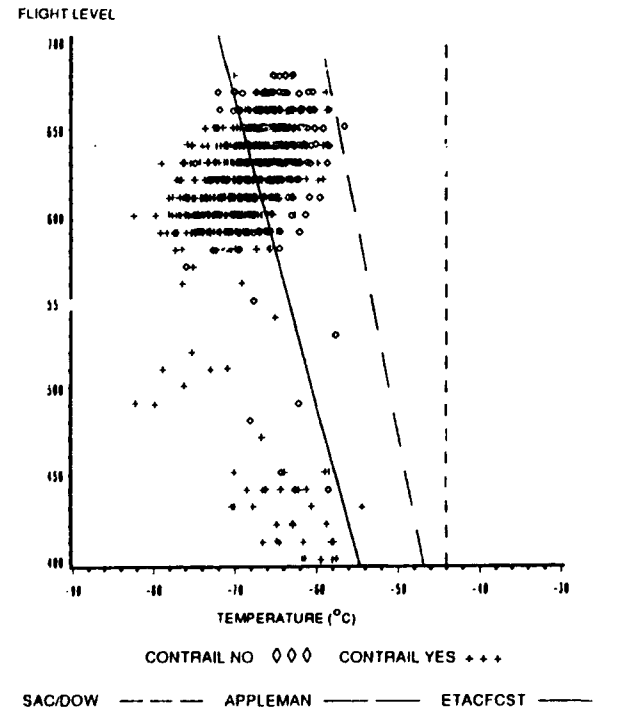


**Figure 12.** Scatter diagram: All PIREP data above 40,000 feet, *RH=100%* for Appleman and SAC/DOW curves.

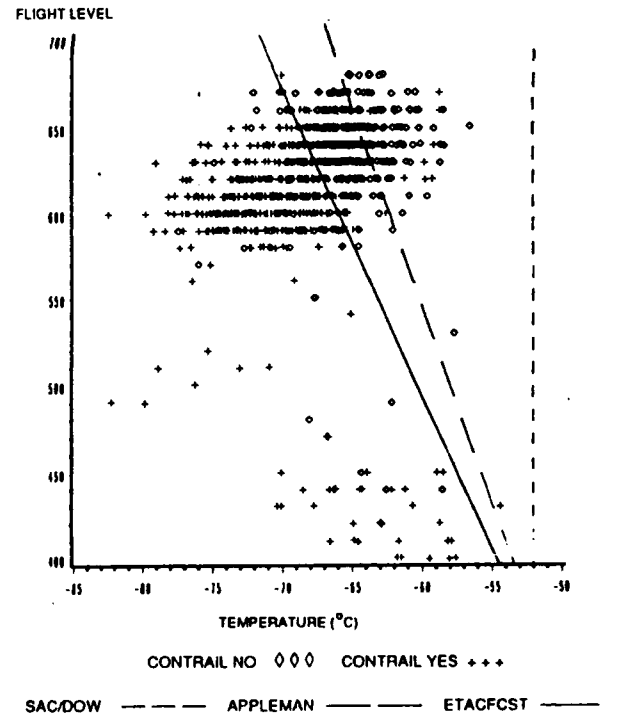


**Figure 13.** Scatter diagram: All PIREP data above 40,000 feet, *RH=10%* for Appleman and SAC/DOW curves.

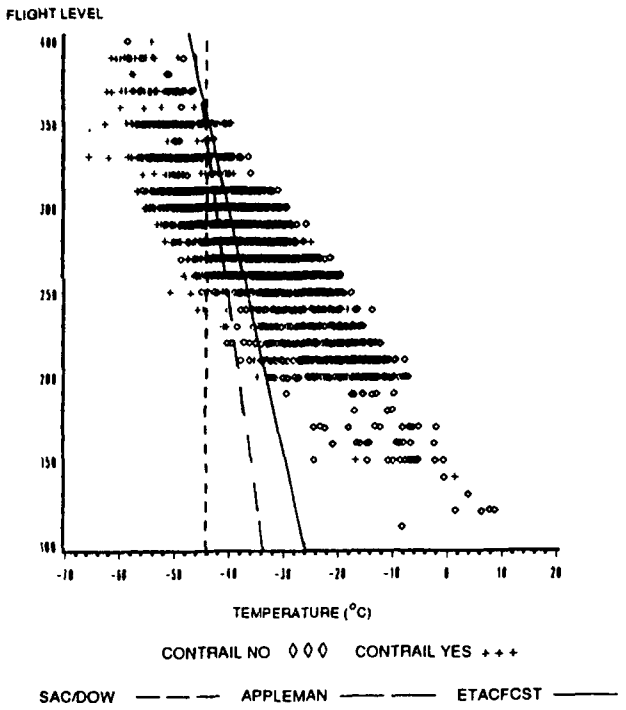


**Figure 14.** Scatter diagram: All HIRAS data at/below 40,000 feet, using *all vertical motion, RH=100%* for appleman and SAC/DOW curves.

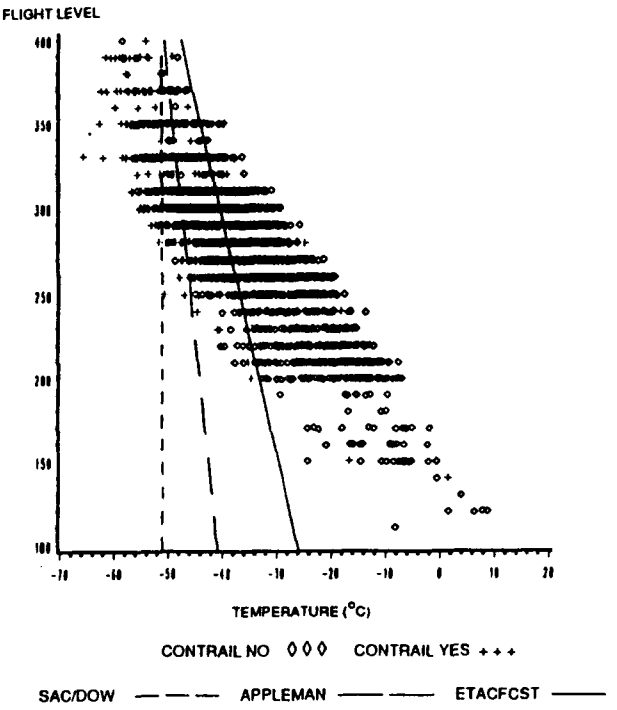


**Figure 15.** Scatter diagram: All HIRAS data at/below 40,000 feet, using *all vertical motion, RH=40%* for appleman and SAC/DOW curves.

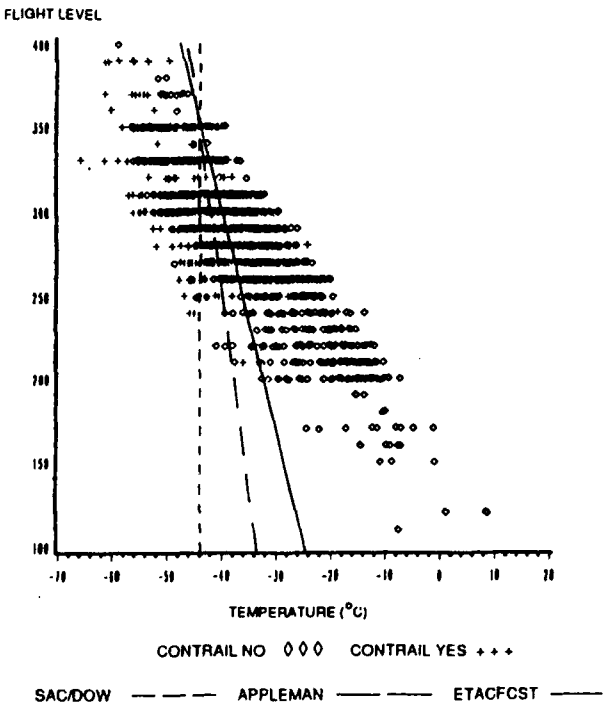


**Figure 16.** Scatter diagram: All HIRAS data at/below 40,000 feet, using *upward vertical motion only, RH=100%* for Appleman and SAC/DOW curves.

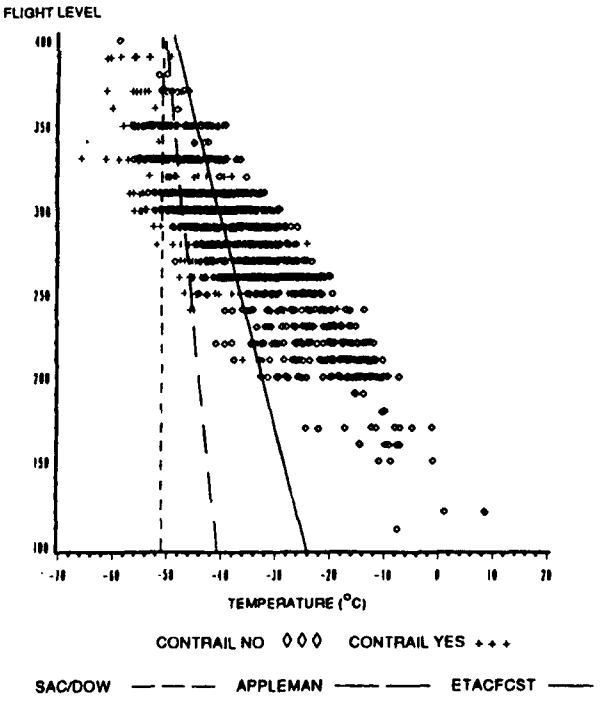


**Figure 17.** Scatter diagram: All HIRAS data at/below 40,000 feet, using *upward vertical motion only*, RH=40% for Appleman and SAC/DOW curves.

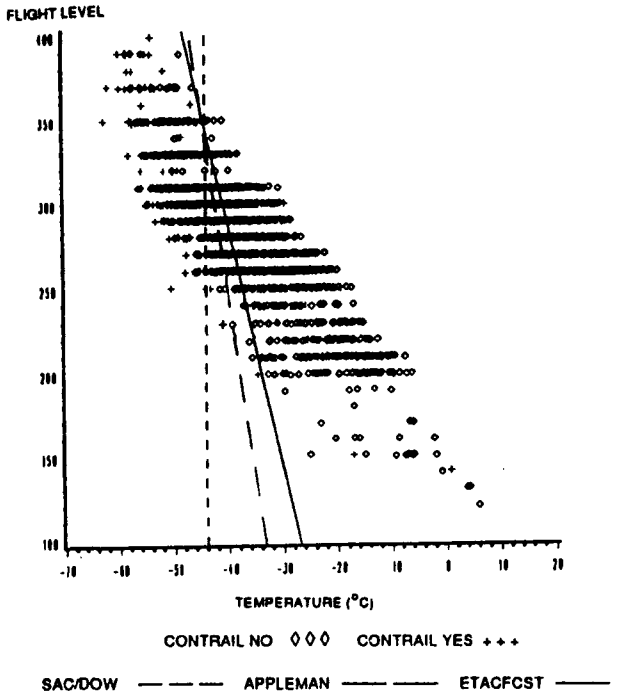


**Figure 18.** Scatter diagram: All HIRAS data at/below 40,000 feet, using *downward vertical motion only, RH=100%* for Appleman and SAC/DOW curves.

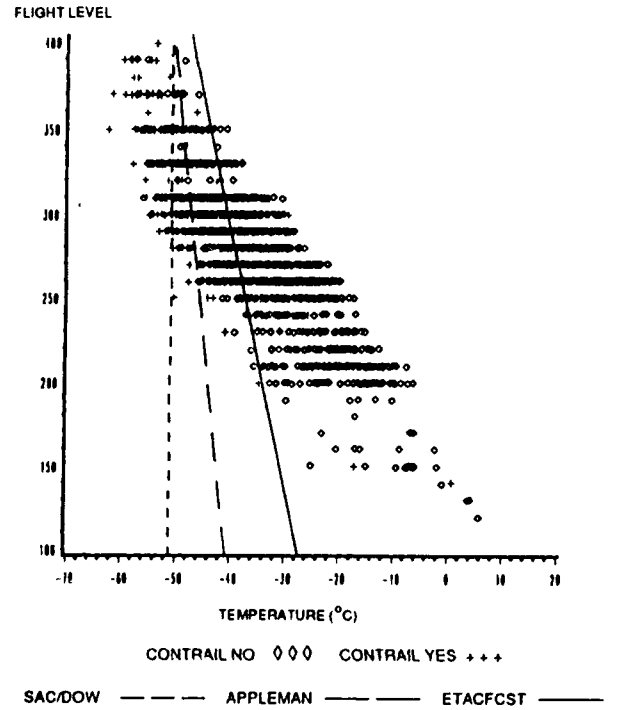


**Figure 19.** Scatter diagram: All HIRAS data at/below 40,000 feet, using *downward vertical motion only, RH=40%* for Appleman and SAC/DOW curves.

***4.4.3 HIRAS Temperature Data At/Below 40,000 Feet.*** Figures 14 through 19 depict contrails as a function of altitude and temperature or altitude, temperature, and vertical motion using calculated HIRAS data. SAC/DOW and Appleman curves are plotted assuming 100 or 40% RH; ETACFCST curves are also plotted based on the following discriminant equations:

$$TCRIT = -18.90 - (0.0717 \times FL) \quad (17)$$

for HIRAS temperatures and upward/downward vertical motion;

$$TCRIT = -16.32 - (0.0793 \times FL) \quad (18)$$

for HIRAS temperatures and upward motion; and

$$TCRIT = -20.39 - (0.0681 \times FL) \quad (19)$$

for HIRAS temperatures and downward motion. *TCRIT* and *FL* represent the temperature (° C) at flight level and flight level (hundreds of feet), respectively. Statistical results (Appendix A, Tables A5-A7) using HIRAS are similar (but slightly inferior) to results using original PIREP data. ETACFCST proves to be the best predictor of contrails, regardless of the sign of the vertical motion. POD is considerably higher for ETACFCST than for Appleman or SAC/DOW, but the FAR is also higher. The discriminant V-score indicates moderate skill for ETACFCST and low skill for Appleman and SAC/DOW, regardless of the sign of vertical motion.

***4.4.4 HIRAS Data in 5,000- or 6,000-Foot Increments Between FL 200 and 400.*** HIRAS data was separated into three 5,000-foot bins and one 6,000-foot bin between 20,000 and 40,000 foot by flight level, as shown below:

- FL 200 and 240
- FL 250 and 290
- FL 300 and 340
- FL 350 and 400.

*4.4.4.1 Upward/Downward Vertical Motion (All Motions).* The discriminant equations (with resulting statistics) using all vertical motion data are shown in Appendix B, Table B-1. The slope of the discriminant curve decreases (becomes more negative) with increasing flight level. Below FL 250, the slope is positive, which indicates that contrail frequency increases with increasing temperature. This finding is not supported by physics or statistics, which indicate poor skill, FAR, and POD. All statistics improve considerably between FL 200 and 240 and between FL 350 and 400. In general, there is some improvement in forecasting contrails using this method (i.e., separate discriminant equation every 5,000 feet) compared to one discriminant curve for all data at/below 40,000 feet (compare Tables A-5 and B-1). Furthermore, this method is slightly better than results obtained when applying the same discriminant curve (Equation 17) for each 5,000-foot increment of data at or below 40,000 feet (compare Table A-5 with Table C-1 of Appendix C). However, this improvement at many layers is a statistical artifact of having fewer data points to fit; i.e., two opposite categorical data points will always produce a perfect discriminant analysis solution.

*4.4.4.2 Upward Vertical Motion.* The discriminant equations (with statistics) using HIRAS upward motion data are shown in Appendix B, Table B-2. Little, if any, improvement is noted by using separate discriminant equations every 5,000 feet between FL 200 and 400 (Table B-2), compared to using one discriminant equation (Equation 18) for all data at/below 40,000 feet (Table A-6) or applying the same equation (18) to each 5,000-foot increment between FL 200 and 400 (Appendix C, Table C-2). Although skill and POD are slightly lower for each 5,000-foot increment (Table B-2) than for ETACFCST (Table A-6), POD does improve considerably between FL 350 and 400 (Table B-2).

*4.4.4.3 Downward Vertical Motion.* Table B-3 depicts the discriminant equations and associated statistics using HIRAS downward vertical motion data. Slopes decrease (become more negative) with increasing flight level up to 34,000 feet, then increase slightly between FL 350 and 400. Statistics show favorable results, especially above FL 300. This method offers some improvement over the use of a single discriminant equation (19) for all data at/below 40,000 feet (compare Tables A-7 and B-3) or over the use of a single equation (19) for data in 5,000-foot increments at/below 40,000 feet (Table C-3). This is especially true above 35,000 feet, where skills are relatively high and the false alarm rate is low.

**4.5 Comparison with Data from Previous Study.** Data used by Miller (1990) was run through the same software used to create statistics associated with the ETACFCST, SAC/DOW, and Appleman techniques. The data was limited to altitudes of 40,000 feet or less. ETACFCST software was based on discriminant curves using PIREP and HIRAS temperature and all vertical motion data (Equations 13 and 17, respectively). Results for the different curves were unimpressive. Although ETACFCST had a high POD (94% using PIREP data or 88% with HIRAS data) and low FAR (7% using PIREP or HIRAS data), two skill scores indicated little skill (VDS=0.11 and 0.03; HSS=0.00 and 0.03 using PIREP or HIRAS data, respectively). The CSI, however, did indicate high skill (CSI=0.88). SAC/DOW and Appleman curves were equally unimpressive. Both had equal or slightly better skill than ETACFCST, but the POD was 10 to 20% less. The poor skill for all the curves is primarily the result of the inability to forecast non-occurrences of contrails.

**4.6 ETACFCST Curve Comparison.** ETACFCST contrail prediction curves based on original PIREP and calculated HIRAS data were compared for upward, downward, and all vertical motions. Slopes of the discriminant curves were similar (compare slopes in Equations 14 and 17, 15 and 18, 16 and 19). For example, slopes of HIRAS and PIREP upward motion discriminant curves were 0.079 and 0.049, respectively. At 40,000 feet, the critical temperature varies by 2

to 7° C due to the change in slope of the discriminant curves. About 73% (1,524 of 2,093) of the PIREPs associated with upward motion were correctly forecast; 68% (1,361 of 2,002) were correctly forecast using HIRAS data. For downward motion, percent correct was about 69% for both PIREP and HIRAS data. Similarly, results indicate that although HIRAS temperatures replaced PIREP temperatures in about 60% of all dependent observations, there was very little difference in the discriminant curves using HIRAS (or PIREP) temperatures with HIRAS or PIREP vertical motions. For example, comparing results using PIREP temperature and upward vertical motion data with HIRAS temperature and PIREP upward vertical motion data, the slope of the discriminant equation ranged from 0.050 to 0.075, respectively; percent correct differed by less than 1% (only 19 of 2,093 correct forecasts differed). Thus, it appears the biggest changes (although small) in slope (and percent correct) occurs when comparing results from the different methods used to calculate vertical velocity.

**4.7 Independent Testing.** We kept 1,341 observations for independent testing; 1,110 occurred at/below 40,000 feet, 231 above 40,000 feet. Results of the tests are shown in the tables of Appendices A, B, and C. In general, results support ETACFCST as the most skillful of the three contrail prediction curves. POD, FAR, and COR were similar to results using the dependent data (described above). Based on these results, ETACFCST may be a satisfactory method for predicting contrails at **any** flight level above 25,000 feet.

**4.8 AFGWC Results as Tabulated by SAC/DOW.** SAC/DOW provided results of the AFGWC contrail analysis forecast results using the Appleman technique (hit or miss) in the PIREP database. USAFETAC generated and compared statistics using the "hit/miss" data to statistics provided in Table A-1 (see Appleman category in dependent test). In general, statistics were similar. Below 40,000 feet, all three skill scores (VDS, HSS, and CSI) in Table A-1 were within 0.06 of the skill scores computed using the SAC/DOW provided hit/miss data (e.g., HSS = 0.33 from Table A-1 as compared to 0.31 using AFGWC's hit/miss data). The percent correct was within 1% and the false alarm rate and probability of detection were within 10% of the scores obtained using the SAC/DOW results. Above 40,000 feet, all statistics (Table A-4, Appleman category) were easily within 10% of the statistics calculated using SAC/DOW provided hit/miss data. Our implementation of the Appleman technique, therefore, appears to be consistent with AFGWC.

**4.9 Discriminant Analysis Using Engine-Specific Data.** The USAFETAC empirical technique for forecasting contrails scored much higher than the new SAC/DOW theoretical technique when using B-52G data (Appendix D, Table D-1) and slightly higher using KC-135R data (Table D-2). There was little difference between the two techniques when using KC-135A (Table D-3) or U-2 data (Table D-4). The USAFETAC technique produced better results than SAC/DOW's, probably because USAFETAC did not assume RH as SAC does. Instead, USAFETAC determines a temperature threshold that indirectly accounts for a mean atmosphere RH profile that supports a slightly moister RH profile than those given by Nieman (1977) and used at AFGWC. The profiles are reasonable (60% RH vs 40% at 25,000 feet and 20% RH vs 10% in the stratosphere).

Discriminant analysis was also used to obtain the best-fit curve for contrail formation for <u>all</u> non-bypass engine data (KC-135A and B-52G data combined). The results (Table D-5) indicate good skill, a high probability of detection, and a low false alarm rate.

**Caution:** The algorithm based on U-2 data should be applied at altitudes above 40,000 because all the data in the sample were from above 40,000 feet. On the other hand, algorithms developed from KC-135A, KC-135R, and B-52G data should ***not*** be used to forecast contrails above 40,000 feet because only one

observation in the database was from above that altitude. Since contrails seldom occur between 20,000 and 24,000 feet (they were reported in only 27 of 509 PIREPS in the database), the algorithms work best between 25,000 and 40,000 feet. Note: these results were not tested using an independent data set.

## 5. CONCLUSIONS & RECOMMENDATIONS.

**5.1 Conclusions.** Although HIRAS temperatures replaced PIREP temperatures in about 60% of all dependent observations at/below 40,000 feet, there was very little difference (less than 1% correct), between the discriminant equations and associated statistics using HIRAS or PIREP temperature data with either HIRAS or PIREP vertical motions. Combination algorithms based on USAFETAC's empirical contrail forecasting technique and SAC/DOW's engine classification technique provided better results than either technique used alone. Although Equation 17 (ETACFCST using HIRAS upward/downward vertical motion data) could replace the Appleman algorithm technique as the contrail prediction algorithm used by AFGWC, the engine-specific algorithms are better.

***5.1.1 HIRAS and PIREP vertical motion data*** differed in about 38% of all dependent observations at/below 40,000 feet, even though the methods used to estimate the sign of vertical velocity were different. Over 90% of HIRAS and PIREP vertical velocity differences occurred when the estimated HIRAS vertical velocity was near zero +/- 0.005 $ms^{-1}$. Regardless of the technique, the slopes of the discriminant equations were similar, with only a 2-5% correct difference.

***5.1.2 Contrail frequency using PIREP data*** increased from about 20% at 25,000 feet to 60% at 40,000. The frequency of upward motion PIREPS is significantly greater than frequency of downward motion PIREPS. Contrails occur more frequently at lower temperatures, regardless of the vertical motion, but they occur more frequently at the same temperature when there is upward motion. Above 40,000 feet, contrail frequency decreases from 100% between 410 and 440 feet to about 30% above 65,000 feet. Contrails occur 92% of the time when temperatures are -70° C or less.

***5.1.3 Contrail frequency using HIRAS data*** between FL 250 and 340 was similar to the frequency using PIREP data. Z statistics indicate that the differences in frequency of occurrence between upward and downward vertical motion are generally not significant. Between 350 and 400 feet, contrail frequency was higher for downward than for upward motion, but Z statistics show the difference to be insignificant.

***5.1.4 ETACFCST showed the most skill*** in both dependent and independent tests using PIREP or HIRAS data. Below 40,000 ft, ETACFCST had a significantly higher probability of detection (POD) than either Appleman or SAC/DOW, but the false alarm rate (FAR) was also higher. Appleman was slightly better than SAC/DOW in skill, POD, and FAR. Above 40,000 feet, ETACFCST had better skill, percent correct, and FAR than the other curves, but the POD was about 20% lower than Appleman or SAC/DOW.

***5.1.5 Performing several discriminant analyses*** (every 5,000 feet) between FL 200 and 400 using HIRAS data offered some improvement over the "single" discriminant analysis method, especially when only downward motion data was considered. In general, skill, POD, COR, and FAR improve with increasing flight level. However, we do not recommend these curves be used due to data limitations in their development.

**5.2 Recommendations for Operational Use.** Use USAFETAC's empirical technique (discriminant analysis) in combination with SAC/DOW's engine classification technique to forecast contrails; specifically,

- For aircraft with non-bypass engines flying *at/below* 40,000 ft (KC-135A and B-52G), use the discriminant equation provided in Appendix D, Table D-5.

- For aircraft with non-bypass engines flying *above* 40,000 ft (U-2), use the discriminant equation provided in Table D-4.

- For aircraft with high-bypass engines flying at/below 40,000 ft (KC-135R) use the discriminant equation provided in Table D-2.

- There is not enough data to use empirical techniques below 25,000 ft.

**5.3. Recommendations for Future Algorithm Development.** An independent dataset (to test the engine-specific contrail algorithms) should be obtained. Also, recommend that AWS/XTX arrange for the collection of more engine-specific data with ACC/DOW and AMC/DOW. The new data should be used to refine existing algorithms.

# APPENDIX A

**TABLE A-1. Statistics for PIREP temperature and upward/downward vertical motion data using SAC/DOW, Appleman, and USAFETAC contrail prediction curves.** Dependent and independent data at/below 40,000 feet. VDS--V discriminant score; HSS--Heidke skill score; CSI--Critical skill index, COR--percent correct; FAR--False alarm rate; and POD--Probability of detection.

**DEPENDENT**

| PREDICTION CURVE | VDS | HSS | CSI | COR | FAR | POD |
|---|---|---|---|---|---|---|
| SAC/DOW | 0.17 | 0.23 | 0.18 | 78.0 | 18.0 | 18.8 |
| APPLEMAN | 0.26 | 0.33 | 0.27 | 79.5 | 23.1 | 29.4 |
| ETACFCST | 0.42 | 0.34 | 0.39 | 68.4 | 56.3 | 77.0 |

**INDEPENDENT**

| PREDICTION CURVE | VDS | HSS | CSI | COR | FAR | POD |
|---|---|---|---|---|---|---|
| SAC/DOW | 0.13 | 0.18 | 0.15 | 73.9 | 23.1 | 15.4 |
| APPLEMAN | 0.23 | 0.28 | 0.25 | 75.6 | 27.9 | 27.1 |
| ETACFCST | 0.43 | 0.36 | 0.42 | 68.6 | 52.2 | 78.8 |

**TABLE A-2. Statistics for PIREP temperature and upward vertical motion data using SAC/DOW, Appleman, and USAFETAC contrail prediction curves.** Dependent and independent data at/below 40,000 feet. VDS--V discriminant score; HSS--Heidke skill score; CSI--Critical skill index; COR--percent correct; FAR--False alarm rate; and POD--Probability of detection.

**DEPENDENT**

| PREDICTION CURVE | VDS | HSS | CSI | COR | FAR | POD |
|---|---|---|---|---|---|---|
| SAC/DOW | 0.13 | 0.16 | 0.14 | 69.3 | 13.5 | 14.1 |
| APPLEMAN | 0.21 | 0.25 | 0.23 | 71.8 | 16.1 | 23.6 |
| ETACFCST | 0.48 | 0.45 | 0.50 | 72.8 | 41.8 | 78.1 |

**INDEPENDENT**

| PREDICTION CURVE | VDS | HSS | CSI | COR | FAR | POD |
|---|---|---|---|---|---|---|
| SAC/DOW | 0.10 | 0.11 | 0.11 | 59.1 | 15.4 | 11.6 |
| APPLEMAN | 0.19 | 0.20 | 0.21 | 63.1 | 11.1 | 21.1 |
| ETACFCST | 0.38 | 0.37 | 0.54 | 67.6 | 39.8 | 83.7 |

**TABLE A-3. Statistics for PIREP temperature and downward vertical motion data using SAC/DOW, Appleman, and USAFETAC contrail prediction curves.** Dependent and independent data at/below 40,000 feet. VDS--V discriminant score; HSS--Heidke skill score; CSI--Critical skill index; COR--percent correct; FAR--False alarm rate; and POD--Probability of detection.

**DEPENDENT**

| PREDICTION CURVE | VDS | HSS | CSI | COR | FAR | POD |
|---|---|---|---|---|---|---|
| SAC/DOW | 0.26 | 0.35 | 0.26 | 86.0 | 22.8 | 28.2 |
| APPLEMAN | 0.38 | 0.45 | 0.35 | 86.6 | 30.6 | 41.7 |
| ETACFCST | 0.45 | 0.30 | 0.31 | 68.8 | 66.6 | 78.7 |

**INDEPENDENT**

| PREDICTION CURVE | VDS | HSS | CSI | COR | FAR | POD |
|---|---|---|---|---|---|---|
| SAC/DOW | 0.23 | 0.29 | 0.24 | 78.7 | 27.0 | 26.2 |
| APPLEMAN | 0.36 | 0.40 | 0.37 | 79.2 | 37.3 | 45.6 |
| ETACFCST | 0.38 | 0.43 | 0.36 | 59.9 | 62.5 | 87.2 |

**TABLE A-4. Statistics for PIREP temperature data (no vertical motion above 40,00 feet) using SAC/DOW, Appleman, and USAFETAC contrail prediction curves.** Dependent and independent data above 40,000 feet. VDS--V discriminant score; HSS--Heidke skill score; CSI--Critical skill index; COR--percent correct; FAR--False alarm rate; and POD--Probability of detection.

**DEPENDENT**

| PREDICTION CURVE | VDS | HSS | CSI | COR | FAR | POD |
|---|---|---|---|---|---|---|
| SAC/DOW | 0.00 | 0.00 | 0.61 | 60.6 | 39.4 | 100. |
| APPLEMAN | 0.47 | 0.50 | 0.71 | 77.4 | 23.8 | 91.4 |
| ETACFCST | 0.60 | 0.67 | 0.67 | 79.1 | 11.6 | 75.4 |

**INDEPENDENT**

| PREDICTION CURVE | VDS | HSS | CSI | COR | FAR | POD |
|---|---|---|---|---|---|---|
| SAC/DOW | 0.00 | 0.00 | 0.71 | 71.4 | 28.6 | 100. |
| APPLEMAN | 0.41 | 0.44 | 0.75 | 78.8 | 17.8 | 82.2 |
| ETACFCST | 0.51 | 0.44 | 0.65 | 73.2 | 10.1 | 70.3 |

**TABLE A-5. Statistics for HIRAS temperature and upward/downward vertical motion data using SAC/DOW, Appleman, and USAFETAC contrail prediction curves.** Dependent and independent data at/below 40,000 feet. VDS--V discriminant score; HSS--Heidke skill score; CSI--Critical skill index; COR--percent correct; FAR--False alarm rate; and POD--Probability of detection.

**DEPENDENT**

| PREDICTION CURVE | VDS | HSS | CSI | COR | FAR | POD |
|---|---|---|---|---|---|---|
| SAC/DOW | 0.16 | 0.22 | 0.17 | 77.5 | 22.1 | 18.1 |
| APPLEMAN | 0.25 | 0.31 | 0.26 | 79.1 | 23.7 | 27.8 |
| ETACFCST | 0.41 | 0.33 | 0.38 | 68.5 | 56.3 | 75.1 |

**INDEPENDENT**

| PREDICTION CURVE | VDS | HSS | CSI | COR | FAR | POD |
|---|---|---|---|---|---|---|
| SAC/DOW | 0.17 | 0.17 | 0.15 | 73.7 | 25.4 | 15.4 |
| APPLEMAN | 0.26 | 0.26 | 0.23 | 75.6 | 24.0 | 24.3 |
| ETACFCST | 0.45 | 0.38 | 0.43 | 69.8 | 51.0 | 78.8 |

**TABLE A-6. Statistics for HIRAS temperature and upward vertical motion data using SAC/DOW, Appleman, and USAFETAC contrail prediction curves.** Dependent and independent data at/below 40,000 feet. VDS--V discriminant score; HSS--Heidke skill score; CSI--Critical skill index; COR--percent correct; FAR--False alarm rate; and POD--Probability of detection.

**DEPENDENT**

| PREDICTION CURVE | VDS | HSS | CSI | COR | FAR | POD |
|---|---|---|---|---|---|---|
| SAC/DOW | 0.15 | 0.21 | 0.16 | 76.7 | 20.9 | 17.0 |
| APPLEMAN | 0.23 | 0.29 | 0.24 | 78.3 | 21.7 | 25.7 |
| ETACFCST | 0.38 | 0.32 | 0.37 | 68.0 | 56.1 | 71.5 |

**INDEPENDENT**

| PREDICTION CURVE | VDS | HSS | CSI | COR | FAR | POD |
|---|---|---|---|---|---|---|
| SAC/DOW | 0.13 | 0.13 | 0.11 | 72.8 | 24.0 | 11.6 |
| APPLEMAN | 0.22 | 0.24 | 0.20 | 75.5 | 15.0 | 20.7 |
| ETACFCST | 0.46 | 0.40 | 0.44 | 71.0 | 49.4 | 78.1 |

**TABLE A-7. Statistics for HIRAS temperature and downward vertical motion data using SAC/DOW, Appleman, and USAFETAC contrail prediction curves.** Dependent and independent data at/below 40,000 feet. VDS--V discriminant score; HSS--Heidke skill score; CSI--Critical skill index; COR--percent correct; FAR--False alarm rate; and POD--Probability of detection.

**DEPENDENT**

| PREDICTION CURVE | VDS | HSS | CSI | COR | FAR | POD |
|---|---|---|---|---|---|---|
| SAC/DOW | 0.17 | 0.23 | 0.18 | 78.2 | 23.1 | 19.1 |
| APPLEMAN | 0.26 | 0.33 | 0.27 | 79.8 | 25.6 | 30.0 |
| ETACFCST | 0.45 | 0.35 | 0.39 | 69.3 | 56.2 | 78.7 |

**INDEPENDENT**

| PREDICTION CURVE | VDS | HSS | CSI | COR | FAR | POD |
|---|---|---|---|---|---|---|
| SAC/DOW | 0.16 | 0.21 | 0.18 | 74.6 | 26.2 | 19.3 |
| APPLEMAN | 0.23 | 0.28 | 0.25 | 75.6 | 29.7 | 28.0 |
| ETACFCST | 0.47 | 0.39 | 0.44 | 70.4 | 50.6 | 80.1 |

# APPENDIX B

**TABLE B-1. Discriminant equations and resulting statistics using HIRAS temperature and upward/downward vertical motion data.** A different curve is determined for each 5,000 ft (or 6,000 ft) increment between 20,000 and 40,000 ft. VDS--V discriminant score; HSS--Heidke skill score; CSI--Critical skill index; COR--percent correct; FAR--False alarm rate; and POD--Probability of detection.

**DISCRIMINANT EQUATIONS**

| | |
|---|---|
| 200/240 | TCRIT = -51.23 + 0.1196 (FL) |
| 250/290 | TCRIT = -31.67 - 0.0185 (FL) |
| 300/340 | TCRIT = -27.01 - 0.0563 (FL) |
| 350/400 | TCRIT = -31.20 - 0.0539 (FL) |

**DEPENDENT**

| PREDICTION CURVE | VDS | HSS | CSI | COR | FAR | POD |
|---|---|---|---|---|---|---|
| 200/240 | 0.24 | 0.06 | 0.08 | 64.4 | 91.4 | 59.3 |
| 250/290 | 0.31 | 0.23 | 0.29 | 65.5 | 66.2 | 65.8 |
| 300/340 | 0.36 | 0.33 | 0.42 | 67.7 | 49.0 | 69.2 |
| 350/400 | 0.42 | 0.41 | 0.61 | 71.3 | 21.5 | 72.9 |

**INDEPENDENT**

| PREDICTION CURVE | VDS | HSS | CSI | COR | FAR | POD |
|---|---|---|---|---|---|---|
| 200/240 | 0.17 | 0.07 | 0.12 | 65.4 | 87.0 | 50.0 |
| 250/290 | 0.34 | 0.41 | 0.33 | 66.8 | 60.8 | 67.9 |
| 300/340 | 0.41 | 0.38 | 0.47 | 69.2 | 44.3 | 75.5 |
| 350/400 | 0.29 | 0.27 | 0.62 | 69.2 | 20.0 | 75.7 |

**TABLE B-2. Discriminant equations and resulting statistics using HIRAS temperature and upward vertical motion data.** A different curve is determined for each 5,000 ft (or 6,000 ft) increment between 20,000 and 40,000 ft. VDS--V discriminant score; HSS--Heidke skill score; CSI--Critical skill index; COR--percent correct; FAR--False alarm rate; and POD--Probability of detection.

**DISCRIMINANT EQUATIONS**

| | |
|---|---|
| 200/240 | TCRIT = -50.06 + 0.1166 (FL) |
| 250/290 | TCRIT = -33.47 - 0.0097 (FL) |
| 300/340 | TCRIT = -33.02 - 0.0352 (FL) |
| 350/400 | TCRIT = -40.09 - 0.0302 (FL) |

**DEPENDENT**

| PREDICTION CURVE | VDS | HSS | CSI | COR | FAR | POD |
|---|---|---|---|---|---|---|
| 200/240 | 0.08 | 0.02 | 0.06 | 60.9 | 93.3 | 46.2 |
| 250/290 | 0.32 | 0.26 | 0.32 | 67.1 | 61.6 | 64.3 |
| 300/340 | 0.33 | 0.30 | 0.39 | 66.7 | 50.6 | 66.2 |
| 350/400 | 0.30 | 0.29 | 0.52 | 65.1 | 29.1 | 66.1 |

**INDEPENDENT**

| PREDICTION CURVE | VDS | HSS | CSI | COR | FAR | POD |
|---|---|---|---|---|---|---|
| 200/240 | 0.21 | 0.08 | 0.04 | 61.1 | 86.4 | 60.0 |
| 250/290 | 0.30 | 0.25 | 0.32 | 67.2 | 60.0 | 60.0 |
| 300/340 | 0.43 | 0.40 | 0.47 | 70.4 | 44.1 | 75.6 |
| 350/400 | 0.21 | 0.21 | 0.55 | 63.0 | 29.4 | 70.6 |

**TABLE B-3. Discriminant equations and resulting statistics using HIRAS temperature and downward vertical motion data.** A **different** curve is determined for each 5,000 ft (or 6,000 ft) increment between 20,000 and 40,000 ft. VDS--V discriminant score; HSS--Heidke skill score; CSI--Critical skill index; COR--percent correct; FAR--False alarm rate; and POD--Probability of detection.

**DISCRIMINANT EQUATIONS**

| | |
|---|---|
| 200/240 | TCRIT = -51.00 + 0.1158 (FL) |
| 250/290 | TCRIT = -28.62 - 0.0320 (FL) |
| 300/340 | TCRIT = -20.37 - 0.0795 (FL) |
| 350/400 | TCRIT = -27.26 - 0.0678 (FL) |

**DEPENDENT**

| PREDICTION CURVE | VDS | HSS | CSI | COR | FAR | POD |
|---|---|---|---|---|---|---|
| 200/240 | 0.40 | 0.11 | 0.10 | 68.5 | 89.3 | 71.4 |
| 250/290 | 0.32 | 0.22 | 0.27 | 65.2 | 69.0 | 67.9 |
| 300/340 | 0.39 | 0.36 | 0.43 | 68.7 | 47.6 | 71.9 |
| 350/400 | 0.50 | 0.49 | 0.67 | 75.6 | 16.2 | 76.5 |

**INDEPENDENT**

| PREDICTION CURVE | VDS | HSS | CSI | COR | FAR | POD |
|---|---|---|---|---|---|---|
| 200/240 | 0.16 | 0.08 | 0.12 | 70.9 | 86.4 | 42.9 |
| 250/290 | 0.41 | 0.30 | 0.35 | 65.9 | 61.7 | 78.9 |
| 300/340 | 0.32 | 0.30 | 0.43 | 65.1 | 47.2 | 69.1 |
| 350/400 | 0.40 | 0.24 | 0.73 | 72.0 | 11.1 | 80.0 |

# APPENDIX C

**TABLE C-1. Statistics for HIRAS temperature and upward/downward vertical motion data using Equation 17. Data are placed in 5,000 ft (or 6,000 ft) increments as shown.** VDS--V discriminant score; HSS--Heidke skill score; CSI--Critical skill index; COR--percent correct; FAR--False alarm rate; and POD--Probability of detection.

**DEPENDENT**

| PREDICTION CURVE | VDS | HSS | CSI | COR | FAR | POD |
|---|---|---|---|---|---|---|
| 200/240 | 0.22 | 0.24 | 0.16 | 92.7 | 70.8 | 25.9 |
| 250/290 | 0.35 | 0.29 | 0.31 | 71.6 | 61.0 | 60.8 |
| 300/340 | 0.27 | 0.21 | 0.39 | 56.7 | 57.8 | 83.0 |
| 350/400 | 0.14 | 0.16 | 0.63 | 65.7 | 35.6 | 97.1 |

**INDEPENDENT**

| PREDICTION CURVE | VDS | HSS | CSI | COR | FAR | POD |
|---|---|---|---|---|---|---|
| 200/240 | 0.03 | 0.31 | 0.21 | 91.7 | 40.0 | 33.3 |
| 250/290 | 0.38 | 0.34 | 0.36 | 72.2 | 55.4 | 63.4 |
| 300/340 | 0.32 | 0.27 | 0.45 | 60.0 | 52.6 | 89.0 |
| 350/400 | 0.13 | 0.17 | 0.74 | 75.0 | 26.0 | 100. |

**TABLE C-2. Statistics for HIRAS temperature and upward vertical motion data using Equation 18. Data are placed in 5,000 ft (or 6,000 ft) increments as shown.** VDS--V discriminant score; HSS--Heidke skill score; CSI--Critical skill index; COR--percent correct; FAR--False alarm rate; and POD--Probability of detection.

**DEPENDENT**

| PREDICTION CURVE | VDS | HSS | CSI | COR | FAR | POD |
|---|---|---|---|---|---|---|
| 200/240 | 0.24 | 0.20 | 0.14 | 89.7 | 79.0 | 30.8 |
| 250/290 | 0.35 | 0.32 | 0.34 | 72.9 | 55.5 | 57.7 |
| 300/340 | 0.24 | 0.20 | 0.37 | 56.5 | 58.6 | 77.8 |
| 350/400 | 0.15 | 0.17 | 0.60 | 63.1 | 38.5 | 94.9 |

**INDEPENDENT**

| PREDICTION CURVE | VDS | HSS | CSI | COR | FAR | POD |
|---|---|---|---|---|---|---|
| 200/240 | 0.60 | 0.73 | 0.60 | 96.3 | 0.00 | 60.0 |
| 250/290 | 0.34 | 0.32 | 0.34 | 72.7 | 53.5 | 55.0 |
| 300/340 | 0.40 | 0.32 | 0.47 | 63.5 | 51.0 | 91.5 |
| 350/400 | 0.10 | 0.13 | 0.65 | 66.7 | 34.6 | 100. |

**TABLE C-3. Statistics for HIRAS temperature and downward vertical motion data using Equation 19. Data are placed in 5,000 ft (or 6,000 ft) increments as shown.** VDS--V discriminant score; HSS--Heidke skill score; CSI--Critical skill index; COR--percent correct; FAR--False alarm rate; and POD--Probability of detection.

**DEPENDENT**

| PREDICTION CURVE | VDS | HSS | CSI | COR | FAR | POD |
|---|---|---|---|---|---|---|
| 200/240 | 0.20 | 0.24 | 0.16 | 94.2 | 62.5 | 21.4 |
| 250/290 | 0.38 | 0.31 | 0.31 | 73.5 | 62.2 | 61.5 |
| 300/340 | 0.27 | 0.21 | 0.40 | 55.4 | 57.9 | 88.0 |
| 350/400 | 0.12 | 0.14 | 0.66 | 67.7 | 33.3 | 98.8 |

**INDEPENDENT**

| PREDICTION CURVE | VDS | HSS | CSI | COR | FAR | POD |
|---|---|---|---|---|---|---|
| 200/240 | 0.00 | 0.00 | 0.00 | 88.6 | 100. | 0.00 |
| 250/290 | 0.48 | 0.41 | 0.40 | 75.7 | 52.0 | 71.2 |
| 300/340 | 0.25 | 0.21 | 0.43 | 55.8 | 54.4 | 88.9 |
| 350/400 | 0.20 | 0.29 | 0.83 | 84.0 | 16.7 | 100. |

# APPENDIX D

**TABLE D-1. Comparison of the ETAC empirical and SAC/DOW theoretical contrail prediction algorithms using B-52G data (340 observations).** VDS--Discriminant V Skill Score; FAR--False Alarm Rate; POD--Probability of Detection. OCCUR: Forecast occurrence of contrails. NON-OCCUR: Forecast non-occurrence of contrails. Also shown is the ETAC discriminant equation (TCRIT is the critical temperature for contrail formation in degrees celsius; FL is flight level in hundreds of feet (i.e., 200 = 20,000 ft).

**B-52G NON BY-PASS ENGINE**

| | ETAC | SAC/DOW |
|---|---|---|
| VDS | 0.55 | 0.37 |
| OCCUR | | |
| POD | 79 | 40 |
| FAR | 30 | 5 |
| NON-OCCUR | | |
| POD | 77 | 98 |
| FAR | 16 | 43 |

TCRIT = 3.47 - 0.152 (FL)

**TABLE D-2. Comparison of the ETAC empirical and SAC/DOW theoretical contrail prediction algorithms using KC-135R data (332 observations).** VDS--Discriminant V Skill Score; FAR--False Alarm Rate; POD--Probability of Detection. OCCUR: Forecast occurrence of contrails. NON-OCCUR: Forecast non-occurrence of contrails. Also shown is the ETAC discriminant equation (TCRIT is the critical temperature for contrail formation in degrees celsius; FL is flight level in hundreds of feet (i.e., 200 = 20,000 ft)).

**KC-135R HIGH BY-PASS ENGINE**

| | ETAC | SAC/DOW |
|---|---|---|
| VDS | 0.58 | 0.53 |
| OCCUR | | |
| POD | 83 | 71 |
| FAR | 28 | 22 |
| NON-OCCUR | | |
| POD | 75 | 82 |
| FAR | 15 | 24 |

TCRIT = -9.45 - 0.105 (FL)

**TABLE D-3. Comparison of the ETAC empirical and SAC/DOW theoretical contrail prediction algorithms using KC-135A data (322 observations).** VDS--Discriminant V Skill Score; FAR--False Alarm Rate; POD--Probability of Detection. OCCUR: Forecast occurrence of contrails. NON-OCCUR: Forecast non-occurrence of contrails. Also shown is the ETAC discriminant equation (TCRIT is the critical temperature for contrail formation in degrees celsius; FL is flight level in hundreds of feet (i.e., 200 = 20,000 ft)).

**KC135-A NON BY-PASS ENGINE**

| | ETAC | SAC/DOW |
|---|---|---|
| VDS | 0.48 | 0.46 |
| OCCUR | | |
| POD | 79 | 61 |
| FAR | 28 | 18 |
| NON-OCCUR | | |
| POD | 69 | 85 |
| FAR | 24 | 34 |

TCRIT = -6.87 - 0.121 (FL)

**TABLE D-4. Comparison of the ETAC empirical and SAC/DOW theoretical contrail prediction algorithms using U-2 data (1022 observations).** VDS--Discriminant V Skill Score; FAR--False Alarm Rate; POD--Probability of Detection. OCCUR: Forecast occurrence of contrails. NON-OCCUR: Forecast non-occurrence of contrails. Also shown is the ETAC discriminant equation (TCRIT is the critical temperature for contrail formation in degrees celsius; FL is flight level in hundreds of feet (i.e., 200 = 20,000 ft)).

**U-2 NON BY-PASS ENGINE**

| | ETAC | SAC/DOW |
|---|---|---|
| VDS | 0.60 | 0.62 |
| OCCUR | | |
| POD | 79 | 75 |
| FAR | 12 | 11 |
| NON-OCCUR | | |
| POD | 70 | 86 |
| FAR | 28 | 31 |

TCRIT = -31.6 - 0.057 (FL)

**TABLE D-5. Comparison of the ETAC empirical and SAC/DOW theoretical contrail prediction algorithms using KC-135A and B-52G data (non by-pass engine; at/below 40,000 ft).** VDS--Discriminant V Skill Score; FAR--False Alarm Rate; POD--Probability of Detection. OCCUR: Forecast occurrence of contrails. NON-OCCUR: Forecast non-occurrence of contrails. Also shown is the ETAC discriminant equation (TCRIT is the critical temperature for contrail formation in degrees celsius; FL is flight level in hundreds of feet (i.e., 200 = 20,000 ft)).

**B-52G and KC-135A, NON BY-PASS ENGINE**

| | ETAC | SAC/DOW |
|---|---|---|
| VDS | 0.51 | N/A |
| OCCUR | | |
| POD | 80 | |
| FAR | 30 | |
| NON-OCCUR | | |
| POD | 81 | |
| FAR | 19 | |

TCRIT = -1.61 - 0.137 (FL)

## BIBLIOGRAPHY


Afifi, A.A., and V. Clark, *Computer-Aided Multivariate Analysis*, Van Nostrand Reinhold Co., 1984.

Appleman, H.S, "A Fallacy in the Use of Skill Scores", *Bull. Amer. Met. Soc.*, 41, 64-67, 1960.

Appleman, H.S, "The Formation of Exhaust Condensation Trails by Jet Aircraft," *Bull. Amer. Met. Soc.*, 34, 14-20, 1953.

Duffield, G.F., and G.D. Nastrom, *Equations and Algorithms for Meteorological Applications in Air Weather Service*, AWS/TR-83/001, HQ Air Weather Service, Scott AFB, IL, 1983.

Goldsmith, B.S., "A Comprehensive Analysis of Verification Results for Forecasts of Precipitation Type and Snow Amount," Paper presented at the 11th Conference on Probability and Statistics, 1989.

Hair J.F., R.E. Anderson, and R.L. Tarthan, *Multivariate Data Analysis*, Van Nostrand Reinhold Co., 1984.

Hanssen, A.W., and W.J.A. Kuipers, "On the Relationship Between the Frequency of Rain and Various Meteorological Parameters", *Koninklijk Nederlands Meteorologisch Institu.*, Meded. Verhand., 81, 2-15, 1968.

List, R.J., *Smithsonian Meteorological Tables*, Sixth Revised Edition, Smithsonian Institution Press, Washington D.C., 1984.

Miller, W.F., *SAC Contrail Forecasting Algorithm Validation Study*, USAFETAC/PR-90/003, USAF Environmental Technical Applications Center, Scott AFB, IL, 1990.

Woodcock, F., "The Evaluation of Yes/No Forecasts for Scientific and Administration Purposes", *Mon. Wea. Rev.*, 104, 1209-1214, 1976.

## ACRINABS

| | |
|---|---|
| AFGWC | Air Force al Weather Central |
| AWAPS | Advanced Weather Analysis and Prediction System |
| $a_1$ | discriminant weight used in discriminant analysis |
| $a_2$ | discriminant weight used in discriminant analysis |
| COR | percent correct |
| CSI | Critical Skill Index |
| DA | Discriminant Analysis |
| $d_x u$ | difference of u-comp horizontal wind in $ms^{-1}$ |
| $d_x v$ | difference of v-comp horizontal wind in $ms^{-1}$ |
| e | exponential |
| ETACFCST | USAFETAC algorithm for forecasting contrails |
| FAR | False Alarm Rate |
| FL | Flight Level in meters |
| FLTLVL | flight level in meters |
| FCST | forecast |
| g | gravity in $ms^{-2}$ |
| HIRAS | High Resolution Analysis System |
| HSS | Heidke Skill Score |
| m | meters |
| mb | millibars |
| $ms^{-1}$ | meters per second |
| N | number of observations |
| NGM | Nested Gridded Model |
| nm | nautical miles |
| OBS | observed |
| P | distance in meters |
| p | pressure in millibars |
| $p_i$ | pressure in millibars at level i |
| $p_{i+1}$ | pressure in millibars at level i+1 |
| PIBAL | PIBAL observation |
| PIREP | Pilot Report |
| POD | Probability of Detection |
| PVAL | p-value |
| QC | quality control |
| R | dry gas constant |
| $\varrho_k$ | density in $kgm^{-3}$ at level k |
| $\varrho_{k-1}$ | density in $kgm^{-3}$ at level k-1 |
| RAOB | Radiosonde observation |
| RH | relative humidity |
| S | interpolated distance in meters |
| SAC | Strategic Air Command |
| SAC/DO | Strategic Air Command, Director of Operations |
| SAC/DOW | Strategic Air Command, Director of Weather |
| T | Temperature in °C at required point or PIREP point |
| $T_i$ | Temperature in °C at grid point i or at pressure $p_i$ |
| $T_{i+1}$ | Temperature in °C at grid point i+1 or at pressure $p_{i+1}$ |

| | |
|---|---|
| $T_p$ | Temperature in °C at latitude/longitude location of PIREP at standard levels above/below each PIREP |
| $T_{S1}$ | Temperature in °C at point S1 |
| $T_{S2}$ | Temperature in °C at point S2 |
| TCRIT | Critical temperature (°C) for formation of contrails |
| TROPFCST | Appleman algorithm for forecasting contrails |
| USAFETAC | USAF Environmental Technical Applications Center |
| VDS | Discriminant V-score |
| $w_k$ | vertical velocity in $ms^{-1}$ half a level above standard level |
| $w_{k-1}$ | vertical velocity in $ms^{-1}$ half a level below standard level |
| Z | discriminant score |
| $Z_M$ | flight level in feet |
| $Z_M$ | flight level in meters |

## DISTRIBUTION

| | |
|---|---|
| USTC J3/J4-OW, Scott AFB, IL 62225-7001 | 1 |
| AWS/XTX, Scott AFB, IL 62225-5008 | 1 |
| Det 3, DOXW, PO Box 95004, Henderson, NV 89009-5004 | 1 |
| Det 4, AWS, Bldg 91027, Hurlburt Fld, FL 32544-5000 | 1 |
| OL-B, HQ AWS, Hanscom AFB, MA 01731-5000 | 1 |
| HQ AFGWC/DO/SY/RM, MBB39, 106 Peacekeeper Dr., Offutt AFB, NE 86113-4039 | 1 |
| OL-A, AFGWC, FLENUMOCEANCEN, Monterey CA 93943-5995 | 1 |
| OL-C, AFGWC, NOAA NESDIS, Federal Bldg 4, Washington, DC 20233-0001 | 1 |
| AFSFC/DOM, Stop 82, Bldg 715, Falcon AFB, CO 80912-5000 | 1 |
| USAFETAC, Scott AFB, IL 62225-5000 | 6 |
| OL-A, USAFETAC, Federal Building, Asheville, NC 28801-2723 | 1 |
| AFSPACECOM/DOW, Stop 7, Peterson AFB, CO 80914-5000 | 1 |
| AFMC(I)/DOW, Wright-Patterson AFB, OH 45433-5000 | 1 |
| FASTC/TAW, Wright-Patterson AFB, OH 45433-6508 | 1 |
| ASD/WE, Bldg 91, Wright-Patterson AFB, OH 45433-6503 | 1 |
| AFIT/CIR, Wright-Patterson AFB, OH 45433-6583 | 1 |
| WL/DOWA, Wright-Patterson AFB, OH 45433-6543 | 1 |
| WL/DOW, Wright Patterson AFB, OH 45433-6543 | 1 |
| FASTC/TAW, Wright-Patterson AFB, OH 45433-6543 | 1 |
| PL/WE, Kirtland AFB, NM 87117-5000 | 1 |
| RL/WE, Griffiss AFB, NY 13441-5700 | 1 |
| RL/DOVL, Bldg 106, Griffiss AFB, NY 13441-5700 | 1 |
| BMO/WE, Norton AFB, CA 92409-6568 | 1 |
| HQ AFCESA/WE, Stop 21, Tyndall AFB, FL 32403-6001 | 1 |
| AFESC/RDXT, Bldg 1120, Stop 21, Tyndall AFB, FL 32403-5000 | 1 |
| ESD/WE, Bldg 1624, Hanscom AFB, MA 01731-5000 | 1 |
| PL/TSML, Research Library, Hanscom AFB, MA 01731-5000 | 1 |
| 3246TW/DOW, Bldg 60, Rm 60, Eglin AFB, FL 32542-5000 | 1 |
| AFFTC/WE, Edwards AFB, CA 93523-5000 | 1 |
| 510 OSS/WE, Bldg 1200, Edwards AFB, CA 93523-5000 | 1 |
| 6585 TG/WE, Holloman AFB, NM 88330-5000 | 1 |
| SSD/SDW, PO Box 92960, Los Angeles AFB, CA 90009-2960 | 1 |
| UTTR/WE, Hill AFB, UT 84056-5000 | 1 |
| 2849 ABG/DOW, Hill AFB, UT 84056-5000 | 1 |
| 2851 ABG/DOW, Bldg 1610, Kelly AFB, TX 78241-5000 | 1 |
| 2852 ABG/DOW, McClellan AFB, CA 95652-5987 | 1 |
| 2853 ABG/DOW, Robins AFB, GA 31098-5000 | 1 |
| 2854 ABG/DOW, L18, Tinker AFB, OK 73145-5000 | 1 |
| USAFA/CWOSW, USAF Academy, CO 80840-5000 | 1 |
| USCENTCOM/J3-W, MacDill AFB, FL 33608-7001 | 1 |
| AFTAC/WS, Patrick AFB, FL 32925-5000 | 1 |
| ESMC/WE, Patrick AFB, FL 32925-5000 | 1 |
| OL-A, AFCOS, Fort Ritchie, MD 21719-5010 | 1 |
| USAFALCENT RA, Pope AFB, NC 28308-5000 | 1 |
| CCSO/FL, Tinker AFB, OK 73145-6340 | 1 |
| 304 ARRS/DOOR, Portland IAP, OR 97218-2797 | 1 |
| OL-AW/SSD, JSC, Air Force Technical Library, Houston, TX 77058-5000 | 1 |
| AFOSR/NL, Bolling AFB, DC 20332-5000 | 1 |
| TFWC/WE, Nellis AFB, NV 89191-5000 | 1 |
| 438 OSS/WXF, Bldg 1907, McGuire AFB, NJ 08641-5000 | 1 |
| 89 OSS/WXF, Andrews AFB, MD 20331-5000 | 1 |
| 437 OSS/WXF, Charleston AFB, SC 29404-5000 | 1 |
| 436 OSS/WXF, Dover AFB, DE 19902-5987 | 1 |
| 317 TAW/WXF, Pope AFB, NC 28308-5500 | 1 |
| 60 OSS/WX, Bldg P4, Travis AFB, CA 94535-5986 | 1 |
| 443 OSS/WXF, Altus AFB, OK 73523-5987 | 1 |
| 375 MAW/WXF, Scott AFB, IL 62225-5000 | 1 |
| 62 OSS/WXF, McChord AFB, WA 98438-5987 | 1 |
| 63 MAW/WXF, Norton AFB, CA 92409-5987 | 1 |
| 314 OSS/WXF, Little Rock AFB, AR 72099-5987 | 1 |
| 542 OSS/WXF, Kirtland AFB, NM 87117-5987 | 1 |

834 OSS/WXF, Hurlburt Field, FL 32544-5000 ..... 1
AFSOC/DOW, Hurlburt AFB, FL 32544-5000 ..... 1
ATC/DOTW, Randolph AFB, TX 78150-5001 ..... 1
3395TCHTS/TTMV, Keesler AFB, MS 39534-5000 ..... 1
Det 5, HQ AWS, Keesler AFB, MS 39534-5000 ..... 1
3340TCHTG/TTGU-W, Stop 16, Chanute AFB, IL 61868-5000 ..... 1
30WS, Unit 15242, APO AP 96205-0015 ..... 1
PACAF/DOW, Hickam AFB, HI 96853-5000 ..... 1
11WS, 6900 9th Ste 205, Elmendorf AFB, AK 99506-5000 ..... 1
USSTRATCOM, J3-15, 901 SAC BLVD, STE BA3, Offutt AFB, NE 68113-5000 ..... 1
22 OSS/DOW, March AFB, CA 92518-5000 ..... 1
90 OSS/DOW, F.E. Warren AFB, WY 82001-5000 ..... 1
55 OSS/DOW, Offutt AFB, NE 68113-5000 ..... 1
93 OSS/DOW, Castle AFB, CA 95342-5000 ..... 1
92 OSS/DOW, Fairchild AFB, WA 99011-5000 ..... 1
301 OSS/DOW, Malmstrom AFB, MT 59402-5000 ..... 1
9 OSS/DOW, Beale AFB, CA 95903-5000 ..... 1
96 OSS/DOW, Dyess AFB, TX 79607-5000 ..... 1
5 OSS/DOW, 221 Flight Line Dr., Minot AFB, MD 58705-5021 ..... 1
384 OSS/DOW, McConnell AFB, KS 67221-5000 ..... 1
2 OSS/DOW, Barksdale AFB, LA 71110-5002 ..... 1
8 AF/DOW, Barksdale AFB, LA 71110-5002 ..... 1
42 OSS/DOW, Loring AFB, ME 04751-5000 ..... 1
416 OSS/DOW, Griffiss AFB, NY 13441-5000 ..... 1
380 OSS/DOW, Plattsburgh AFB, NY 12903-5000 ..... 1
97 OSS/DOW, Eaker AFB, AR 72317-5000 ..... 1
319 OSS/DOW, Grand Forks AFB, ND 58205-5048 ..... 1
28 OSS/DOW, Ellsworth AFB, SD 57706-5000 ..... 1
351 OSS/DOW, Whiteman AFB, MO 65305-5000 ..... 1
7 OSS/DOW, Carswell AFB, TX 76127-5000 ..... 1
410 OSS/DOW, K.I. Sawyer AFB, MI 49843-5000 ..... 1
305 OSS/DOW, Grissom AFB, IN 46971-5000 ..... 1
379 OSS/DOW, Wurtsmith AFB, MI 48753-5000 ..... 1
TAC/DOW, Bldg 21, Langley AFB, VA 23655-5524 ..... 1
5WS, FCWE/SWO, Bldg 168, Ft McPherson, GA 30300-5000 ..... 1
USAFE/DOW, Unit 3050, Box 15, APO AE 09094-5000 ..... 1
USAFE/DOWO, Unit 3050, Box 500, APO AE 09094-5000 ..... 1
17AF/DOW, Unit 4065, APO AE 09136-5000 ..... 1
7WS, CINCUSAREUR/AREAWX, APO AE 09403-5000 ..... 1
COMNAVOCEANCOM, Code N312, Stennis Space Ctr, MS 39529-5000 ..... 2
NAVOCEANO (Rusty Russum), Bldg 8100, Rm 203D, Stennis Space Ctr, MS 39522-5001 ..... 2
NAVOCEANO, Code 9220 (Tony Ortolano), Stennis Space Ctr, MS 39529-5001 ..... 1
Naval Research Laboratory, Monterey, CA 93943-5006 ..... 1
Naval Research Laboratory, Code 4323, Washington, DC 20375 ..... 1
Naval Postgraduate School, Chmn, Dept of Meteorology, Code 63, Monterey, CA 93943-5000 ..... 1
Naval Oceanography Command Ctr, COMNAVMAR Box 12, FPO San Francisco, CA 96630-5000 ..... 1
Naval Oceanography Command Ctr, Box 31, USNAVSTA FPO New York, NY 09540-3000 ..... 1
Naval Air Warfare Center-Weapons Division, Geophysical Sciences Branch, Code 3254, Attn: Mr. Roger Helvey,
Point Mugu, CA 93042-5001 ..... 1
USCINCPAC (J37), Box 13, Camp H.M. Smith, HI 96861-5025 ..... 1
Armed Forces Medical Intelligence Center, Information Services Division
Bldg 1607, Ft Detrick, Frederick, MD 21702-5004 ..... 1
TECOM, Dir for Technology, APG Met Team, Bldg 1134, Attn: AMSTE-TC-AM CAB,
Aberdeen Proving Bround, MD 21005-5001 ..... 1
Atmospheric Sciences Laboratory (SLCAS-AS-I 3 10-2c), White Sands Missile Range, NM 88002-5501 ..... 1
TECOM Atmos Sci Div, AMSTE-TC-AA (MacBlain), White Sands Missile Range, NM 88002-5504 ..... 1
White Sands Met Team, AMSTE-TC-AM (WS), White Sands Missile Range, NM 88002-5501 ..... 1
Army Missile Command, ATTN: AMSMI-RD-TE-F, Redstone Arsenal, AL 35898-5250 ..... 1
USATECOM, ATTN: AMSTE-TC-AM (RE) TCOM Met Team, Redstone Arsenal, AL 35898-8052 ..... 1
USATECOM, ATTN: AMSTE-TC-AM (AB), Aberdeen Proving Ground, MD 21005-5001 ..... 1
Director, U.S.A.-CETEC, Attn: GL-AE (Whitmarsh), Fort Belvoir, VA 22060-5546 ..... 1
Technical Library, Dugway Proving Ground, Dugway, UT 84022-5000 ..... 1

HQ NATO Staff Meteorological Officer lMS/OPS APO AE 09724 ..... 1
NOAA/MASC Library MC5, 325 Broadway, Boulder, CO 80303-3328 ..... 2
NOAA Library-EOC4W5C4, Attn: ACQ, 6009 Executive Blvd, Rockville, MD 20852 ..... 1
NOAA/NESDIS (Attn: Nancy Everson, E/RA22), World Weather Bldg, Rm 703, Washington, DC 20233 ..... 1
NIST Pubs Production, Rm A-405, Admin Bldg, Gaithersburg, MD 20899 ..... 1
NASA-MSFC-ES44, Attn: Dale Johnson, Huntsville, AL 35812-5000 ..... 1
NASA-MSFC-ES44, Attn: Gwenevere Jasper, Huntsville, AL 35812-5000 ..... 1
DTIC-FDAC, Cameron Station, Alexandria, VA 22304-6145 ..... 2
AUL/LSE, Maxwell AFB, AL 36112-5564 ..... 1
AWSTL, Scott AFB, IL 62225-5438 ..... 35